Eberhard Karls Universität Tübingen
Institut für Astronomie und Astrophysik
High Energy Astrophysics Group
Tübingen, Germany

Master's Thesis

Master in Astro and Particle Physics

Spectral Analysis of the Low-Mass X-ray Binary Aql X-1 During the 2023 and 2024 Outbursts Using NICER Data

Urvi Nansi

Eberhard Karls Universität Tübingen
Institut für Astronomie und Astrophysik
High Energy Astrophysics Group
Tübingen, Germany

Master's Thesis

Master in Astro and Particle Physics

Spectral Analysis of the Low-Mass X-ray Binary Aql X-1 During the 2023 and 2024 Outbursts Using NICER Data

Author: Urvi Nansi
Matriculation No.: 6300083
Supervisor: Prof. Andrea Santangelo
Second Supervisor: Dr. Can Güngör
Submission Date: November 6, 2025

Declaration of Originality

Hereby I confirm, Urvi Chandresh Nansi, Matriculation Number: 6300083 , that this assignment is my own work and that I have only sought and used mentioned tools. I have clearly referenced in the text and the bibliography all sources used in the work (printed sources, internet or any other source), including verbatim citations or paraphrases. I am aware of the fact that plagiarism is an attempt to deceit which, in case of recurrence, can result in a loss of test authorization. Furthermore, I confirm that neither this work nor parts of it have been previously, or concurrently, used as an exam work, neither for other courses nor within other exam processes.

Place and date: Tübingen, November 6, 2025

Signature:

Abstract

A detailed spectral and timing analysis of the transient neutron-star low-mass X-ray binary Aql X-1 during its 2023 and 2024 outbursts has been carried out using observations obtained with the Neutron Star Interior Composition Explorer (NICER). These two consecutive outbursts, separated by less than a year, were analyzed to investigate the repeatability and variability of the accretion process under comparable physical conditions.

The cleaned NICER event data were processed using the latest calibration database, and spectra were modeled within the 0.6-10 keV energy range employing the absorbed thermal Comptonization model `tbabs*nthcomp`. The evolution of key spectral parameters, including the photon index (Γ), ($kT_{\rm e}$), and seed-photon temperature (kT_{seed}), was examined throughout the outburst phases. Model-independent diagnostics, namely Color-Color Diagrams (CCDs) and Hardness-Intensity Diagrams (HIDs), were constructed to trace spectral state transitions. A dedicated search for millisecond pulsations near the known 550 Hz spin frequency of Aql X-1 was also performed using a custom Python-based pipeline implementing the Z_n^2 test and bootstrap significance estimation.

Both outbursts were found to exhibit canonical atoll-source behavior, evolving from hard (island) to soft (banana) states and back, with clear hysteresis loops. Progressive spectral softening toward the outburst peaks, characterized by increasing Γ and decreasing $kT_{\rm e}$, was interpreted as evidence of coronal cooling by enhanced soft-photon flux from the inner accretion flow. The 2024 outburst was observed to be shorter in duration and marginally harder at peak compared to that of 2023, indicating variations in the initial disk mass or irradiation efficiency rather than in the fundamental accretion mechanism.

No persistent millisecond pulsations were detected during either event. A 3σ upper limit of approximately 1.5% on the fractional rms amplitude was derived, implying that accretion occurred predominantly through a disk-dominated flow, with any magnetically channeled component being intermittent or weak. The consistency in spectral evolution, hysteresis patterns, and parameter trends between the two outbursts supports a scenario

in which thermal-viscous disk instabilities trigger the outbursts, while the geometry of the corona and irradiation feedback govern their detailed behavior.

Through this analysis, Aql X-1 has been established as a benchmark system for investigating the interaction between the accretion disk, boundary layer, and corona in neutron-star low-mass X-ray binaries. The study shows that high-cadence NICER observations can be used to look at the structure and evolution of accretion flows and magnetospheric coupling over short periods of time.

Zusammenfassung

Eine detaillierte spektrale und zeitliche Analyse des transienten Neutronenstern-Niedrigmassen-Röntgendoppelsterns Aql X-1 während seiner Ausbrüche in den Jahren 2023 und 2024 wurde unter Verwendung von Beobachtungen des *Neutron Star Interior Composition Explorer* (NICER) durchgeführt. Diese beiden aufeinanderfolgenden Ausbrüche, die durch weniger als ein Jahr getrennt waren, wurden analysiert, um die Wiederholbarkeit und Variabilität des Akkretionsprozesses unter vergleichbaren physikalischen Bedingungen zu untersuchen.

Die bereinigten NICER-Ereignisdaten wurden mit der neuesten Kalibrationsdatenbank verarbeitet, und die Spektren wurden im Energiebereich von 0.6-10 keV mit dem absorbierten thermischen Comptonisierungsmodell `tbabs*nthcomp` modelliert. Die Entwicklung der wichtigsten spektralen Parameter, einschließlich des Photonenindex (Γ), der Elektronentemperatur (kT_e) und der Seed-Photonen-Temperatur ($kT_{\rm seed}$), wurde über die verschiedenen Ausbruchsphasen hinweg untersucht. Modellunabhängige Diagnostiken, nämlich Farb-Farb-Diagramme (CCDs) und Härte-Intensitäts-Diagramme (HIDs), wurden erstellt, um spektrale Zustandsübergänge nachzuverfolgen. Außerdem wurde eine gezielte Suche nach Millisekundenpulsationen in der Nähe der bekannten Spinfrequenz von 550 Hz von Aql X-1 mit einer speziell entwickelten Python-basierten Pipeline durchgeführt, die den Z_n^2-Test und eine Bootstrap-Signifikanzabschätzung implementiert.

Beide Ausbrüche zeigten das kanonische Verhalten einer Atoll-Quelle, die sich von harten (Insel-) zu weichen (Bananen-) Zuständen und wieder zurück entwickelte, mit deutlich ausgeprägten Hystereseschleifen. Eine fortschreitende spektrale Aufweichung in Richtung der Ausbruchsmaxima, gekennzeichnet durch einen Anstieg von Γ und eine Abnahme von kT_e, wurde als Hinweis auf eine Abkühlung der Korona durch verstärkte weiche Photonenflüsse aus dem inneren Akkretionsstrom interpretiert. Der Ausbruch von 2024 war kürzer und am Maximum geringfügig härter als der von 2023, was auf Unterschiede in der anfänglichen Scheibenmasse oder der Effizienz der Bestrahlung hindeutet, nicht jedoch auf eine Änderung des grundlegenden Akkretionsmechanismus.

Während keines der Ereignisse wurden persistente Millisekundenpulsationen nachgewiesen. Ein 3σ-Obergrenzwert von etwa 1.5 % für die fraktionelle RMS-Amplitude wurde bestimmt, was darauf hinweist, dass die Akkretion überwiegend durch einen scheibendominierten Fluss erfolgte, wobei eine magnetisch kanalisierten Komponente nur intermittierend oder schwach war. Die Übereinstimmung der spektralen Entwicklung, der Hysteresemuster und der Parametertrends zwischen den beiden Ausbrüchen unterstützt ein Szenario, bei dem thermisch-viskose Scheibeninstabilitäten die Ausbrüche auslösen, während die Geometrie der Korona und die Rückkopplung der Bestrahlung ihr detailliertes Verhalten bestimmen.

Durch diese Analyse wurde Aql X-1 als Referenzsystem zur Untersuchung der Wechselwirkung zwischen Akkretionsscheibe, Grenzschicht und Korona in Neutronenstern-Niedrigmassen-Röntgendoppelsternen etabliert. Die Studie zeigt, dass NICER-Beobachtungen mit hoher zeitlicher Abdeckung genutzt werden können, um die Struktur und Entwicklung von Akkretionsflüssen sowie die magnetosphärische Kopplung über kurze Zeiträume hinweg zu untersuchen.

Acknowledgements

I would like to express my deepest gratitude to my supervisor, Prof. Dr. Andrea Santangelo, for his invaluable guidance, support, and encouragement throughout the course of my thesis. As the head of our research group and with many years of experience in the field of High-Energy Astrophysics (HEA), his expertise and insightful feedback greatly enriched the direction and quality of this work.

I am also sincerely thankful to my tutor, Dr. Pengju Wang, for his unwavering support, patient guidance, and continuous encouragement during this journey. His valuable assistance at every stage of my work was essential to the completion of my thesis. His meticulous approach and constant availability greatly enhanced my understanding and overall learning experience.

I would like to thank the Institut für Astronomie & Astrophysik at Eberhard Karls University of Tübingen for providing the academic infrastructure and resources that made this research possible. I also acknowledge the use of resources and data from the NICER mission, which formed a crucial part of my analysis.

I am deeply grateful to all my professors and tutors from whom I have learned throughout the master's program. The knowledge and insights imparted by them have been invaluable and have contributed immensely to my academic growth.

My heartfelt thanks go to my parents for their unconditional love, understanding, constant support, and unshakable belief in me - they have been my greatest motivation. I am equally grateful to my grandparents, whose blessings and love have always been a source of strength. I would especially like to thank Darshan Mama and Kunjal Mami for their love, unwavering belief, and constant guidance in every possible way. I am also very grateful to Mrunal, Janhavi, and Aayushi for always standing by my side and encouraging me through every step.

Finally, I would like to thank my friends Prutha, Janvi, Sindhu, Soumyadeep, and Parth for their motivation, faith, and support, and for making this journey enjoyable and mem-

orable. I also extend my heartfelt gratitude to my friends in India - Sangeeta, Priya, and Ketaki - for their encouragement, emotional support, and constant positivity that have kept me going throughout this endeavor.

I am eternally grateful to all my near and dear ones whose love and belief continue to inspire me.

Lastly, I am grateful to God for guiding me and giving me the clarity to take the right steps. I am also thankful to myself for enduring and persevering through difficult moments, and for striving continuously to become the best version of who I can be.

A teaching from the Shrimad Bhagavad Gita (2.47) that has guided me throughout this journey is:

"Let not the fruits of action be your motive, nor let your attachment be to inaction."

Contents

List of Figures

List of Tables

Chapter 1

Introduction

1.1 Motivation

X-ray binaries (XRBs); section 2.1 are among the most fascinating and powerful celestial systems, providing an unparalleled opportunity to study the physics of accretion, the behavior of matter under extreme gravity, and the equation of state of dense nuclear material. These systems consist of a compact object, either a neutron star (NS) or a black hole (BH), accreting matter from a companion star through Roche lobe overflow or stellar wind capture. The gravitational potential energy of the infalling matter is converted into X-rays, making these binaries bright sources of high-energy radiation (Frank et al., 2002; Lewin et al., 1995; Done et al., 2007).

Within the family of XRBs, Low Mass X-ray Binaries (LMXBs); section 2.2 are particularly valuable for studying accretion processes. In these systems, the donor star typically has a mass below $2M_{\odot}$ and transfers material through Roche lobe overflow, forming an accretion disk around the compact object. The resulting X-ray emission originates primarily from viscous dissipation within the disk and Comptonization processes occurring in a hot electron corona. Neutron star LMXBs are especially interesting because, unlike black holes, their solid surfaces and magnetic fields introduce additional observational signatures such as type-I X-ray bursts, quasi-periodic oscillations (QPOs), and coherent or intermittent pulsed emission (Galloway et al., 2008; van der Klis, 2006; Hasinger and van der Klis, 1989; Casella et al., 2008).

Transient neutron star LMXBs, like Aquila X-1 (Aql X-1); section 2.5, alternate between quiescent and outburst states. During quiescence, accretion nearly halts, and the source remains faint in X-rays, while during outbursts, accretion resumes at much higher rates, causing the luminosity to increase by several orders of magnitude. These recurrent out-

bursts provide a natural timescale to study accretion physics and state transitions. The physical mechanisms behind these outbursts are generally explained by the Disk Instability Model (DIM), which attributes the variability to changes in ionization states within the accretion disk (Lasota, 2001; Hameury, 2020).

Aql X-1, one of the best-studied transient neutron star LMXBs, exhibits frequent and well-documented outbursts approximately once per year. Its accessibility and recurrent activity make it a benchmark source for understanding the link between spectral states and accretion dynamics. The system's outbursts display canonical transitions between hard and soft spectral states, similar to those observed in black hole binaries, allowing a comparative approach to test accretion models across different compact objects (Campana et al., 2014; Asai et al., 2013; Maitra and Bailyn, 2008).

The advent of high-sensitivity and fast-timing observatories such as the NICER has significantly enhanced our ability to study sources like Aql X-1. NICER's soft X-ray coverage (0.2-12 keV) and large collecting area make it particularly suitable for resolving rapid variability and tracking spectral evolution with high temporal precision. Through NICER's observations, it is possible to probe the evolution of the thermal and Comptonized components during different outburst phases, providing insights into the structure and dynamics of the accretion flow and corona (Gendreau et al., 2016).

Aql X-1 is a transient neutron-star LMXB known to exhibit intermittent millisecond X-ray pulsations during certain outbursts (Casella et al., 2008; Bult et al., 2018). Such pulsations arise when accreting plasma is channeled by the star's magnetic field onto its magnetic poles, producing rotational modulation of the X-ray flux. Detection of these pulsations provides a direct measurement of the neutron star's spin frequency and allows constraints on the magnetic field strength, accretion geometry, and coupling between the magnetosphere and the inner accretion disk.

Aql X-1 is particularly intriguing because its pulsations have been detected only sporadically-lasting for a few hundred seconds in isolated intervals-despite extensive observational coverage. Understanding when and why these pulsations appear or vanish offers critical insight into the transitional behavior between purely accretion-powered and rotation-powered states.

Accreting millisecond X-ray pulsars (AMXPs) form a subclass of neutron-star low-mass X-ray binaries that exhibit coherent pulsations with spin frequencies in the range of 180-620 Hz(Patruno and Watts, 2021). These pulsations are produced when accreted plasma is funneled by the neutron star's magnetic field onto the magnetic poles, generating rotationally modulated X-ray emission. The discovery of such systems provided the long-

sought link between LMXBs and radio millisecond pulsars, confirming that accretion torques can spin neutron stars up to millisecond periods (Wijnands and van der Klis, 1998; Patruno and Watts, 2021).

Aql X-1 is one of the most intriguing members of this class. Although it is not a persistent AMXP, brief episode of coherent 550 Hz pulsations have been reported during some outbursts (Casella et al., 2008). These intermittent signals, lasting only a few hundred seconds, suggest that the magnetic field occasionally channels the accretion flow onto the stellar surface. Understanding when and why these pulsations appear or disappear provides critical insight into the coupling between the disk and magnetosphere, the magnetic-field strength, and the geometry of the accretion column.

In the present work, in addition to the spectral analysis, a systematic search for millisecond pulsations in the 2023 and 2024 NICER outbursts of Aql X-1 has been performed. This dual approach allows the study of both the spectral state evolution and the timing signatures associated with magnetically channeled accretion.

1.2 Objectives

The primary goal of this thesis is to investigate the spectral and temporal evolution of Aql X-1 during its 2023 and 2024 outbursts using observations from the NICER mission. By analyzing two consecutive outbursts separated by a short recurrence interval, it becomes possible to examine both the repeatability and variability of the system's accretion behavior under similar conditions. This comparative study helps reveal how the accretion disk and corona evolve, and whether the outburst mechanism exhibits consistent physical signatures across different events.

The specific objectives of this thesis are outlined as follows:

1. **Spectral Analysis:** To perform detailed spectral modeling of Aql X-1 using an absorbed thermal Comptonization model (`tbabs*nthcomp`) across the 0.6-10 keV range. This includes measuring key parameters such as the photon index (Γ), electron temperature (kT_e), and seed photon temperature (kT_{bb}), which characterize the Comptonizing region and the soft emission component. The evolution of these parameters over the course of the outburst will be examined to track the state transitions.

2. **Color-Color and Hardness-Intensity Diagrams:** To construct CCDs and HIDs to study spectral state transitions. These diagrams provide a model-independent way to visualize the evolution of the source and classify it into canonical states such

as hard, intermediate, and soft (Homan et al., 2001; Muñoz-Darias et al., 2022). The tracks in these diagrams will be compared across both outbursts to identify similarities and differences in spectral evolution.

3. **Temporal and Flux Evolution:** To analyze the temporal evolution of the source flux throughout the outbursts using light curves and to correlate the observed variations with changes in spectral parameters. This will help assess whether changes in the accretion rate directly drive state transitions and whether hysteresis effects are present, as often observed in transient LMXBs.

4. **Comparative Outburst Study:** To perform a comparative analysis of the 2023 and 2024 outbursts to explore whether the outburst morphology, peak luminosity, and spectral evolution patterns are consistent between events. This will shed light on the stability of the accretion mechanism and the potential influence of external factors such as mass transfer rate or magnetic field configuration.

5. **Physical Interpretation:** To interpret the observed spectral behavior in the context of theoretical accretion models, particularly the disk instability model and coronal heating mechanisms. The implications for neutron star surface emission and boundary layer physics will also be discussed.

Through these objectives, the thesis aims to provide a coherent picture of the spectral evolution and accretion dynamics in Aql X-1. The outcomes are expected to contribute to a broader understanding of transient neutron star LMXBs and their role in the unified framework of accreting compact binaries.

1.3 Thesis Outline

This thesis is organized into six chapters, each addressing a specific aspect of the study.

- **Chapter 1: Introduction** - provides the scientific motivation, objectives, and scope of the research. It introduces Aql X-1 as a key system for studying accretion physics in neutron star LMXBs.

- **Chapter 2: Theoretical Background** - reviews the fundamental physics of accretion processes, the classification of X-ray binaries, and the spectral and timing properties of LMXBs. It also covers theoretical models relevant to disk instability and spectral state transitions, along with the role of Comptonization and boundary layer emission.

- **Chapter 3: Data and Methodology** - describes the observational data sets used in this study, focusing on NICER observations of Aql X-1 during its 2023 and 2024 outbursts. It details the data reduction pipeline, background modeling, and spectral fitting techniques employed using `HEASoft` and `XSPEC` software tools.

- **Chapter 4: Results** - presents the key findings from the analysis, including spectral fits, flux evolution, and state transition behavior. CCDs and HIDs are introduced to illustrate the spectral evolution throughout the outbursts.

- **Chapter 5: Discussion** - interprets the results in the context of theoretical models and compares them with previous studies of Aql X-1 and other neutron star LMXBs. Possible explanations for differences between the 2023 and 2024 outbursts are discussed, including changes in accretion rate, disk viscosity, or coronal heating.

- **Chapter 6: Summary and Future Work** - concludes the thesis with a synthesis of the results and their astrophysical implications. It also outlines directions for future research, such as time-resolved spectral studies, polarization measurements, or simultaneous multi-wavelength campaigns to probe disk-jet coupling in Aql X-1.

This flow of chapters ensures a logical progression from theoretical background to observational analysis and interpretation. By systematically studying two consecutive outbursts of Aql X-1, this thesis aims to deepen our understanding of how accretion flows evolve in neutron star LMXBs and to contribute to the ongoing effort to bridge the gap between neutron star and black hole accretion phenomena.

Chapter 2

Scientific Background

2.1 X-ray Binaries

X-ray binaries (XRBs) are systems of two stars in which a compact object, like a neutron star (NS) or a black hole (BH), collects mass from a partner star. During the process of accretion, the gravitational potential energy of the material that is falling in is turned into thermal energy and radiation, which makes a lot of X-rays., producing strong X-ray emission. In most systems, this occurs via the formation of an accretion disk, where viscous processes transport angular momentum outward and mass inward. The resulting luminosity can vary widely, typically between 10^{36} and 10^{39} erg s^{-1}, making XRBs some of the brightest X-ray sources in the Galaxy (Bahramian and Degenaar, 2023). They also show variability across a broad range of timescales, from milliseconds (linked to processes in the innermost regions near the compact object) to months or years (set by binary orbital dynamics or disk instabilities).

Based on the mass of the donor star, XRBs are broadly divided into two categories: High-mass X-ray Binaries (HMXBs) and Low-mass X-ray Binaries (LMXBs). In HMXBs, the companion is usually an OB-type massive star, and most of the mass transfer happens through stellar winds. In contrast, in LMXBs the donor star has a mass $\lesssim 1\,M_{\odot}$ and usually fills its Roche lobe, driving mass transfer via Roche-lobe overflow and forming a stable accretion disk (Bahramian and Degenaar, 2023). Because of their luminosity, diversity of states, and accessibility to multi-wavelength observations, XRBs serve as natural laboratories for investigating accretion physics, relativistic effects, and the properties of dense matter in neutron stars.

2.2 Low-Mass X-ray Binaries

LMXBs are the most common type of XRBs in our Galaxy. They have either a neutron star or a black hole that is getting bigger by taking in matter from a low-mass companion. Mass transfer typically occurs via Roche-lobe overflow, creating a geometrically thin, optically thick accretion disk. LMXBs usually have short orbital periods, from a few hours to a few days. However, systems with evolved donors can have longer periods. The spatial distribution of LMXBs within the Milky Way offers significant insights into their origin and evolutionary trajectory. As shown in Figure 2.1, these systems are strongly concentrated toward the Galactic bulge and along the plane. This is because they are linked to the old stellar population. Most LMXBs are found within a few degrees of the Galactic equator. This is in line with the idea that they formed in the dense areas of the inner Galaxy with low-mass donors. The clustering near the Galactic Centre also supports the role of stellar encounters and binary evolution in producing compact X-ray binaries (Sazonov et al., 2020).

LMXBs can be either persistent or transient. Persistent systems accrete steadily and remain bright over long timescales, while transient systems spend most of their lifetimes in quiescence, with luminosities as low as $L_X \sim 10^{33}$ erg s^{-1}, and undergo episodic outbursts where their luminosities rise by several orders of magnitude, up to $L_X \sim 10^{37-38}$ erg s^{-1} (Güngör et al., 2014). These outbursts are understood within the framework of the disk instability model (DIM), where thermal-viscous instabilities in the accretion disk trigger enhanced accretion episodes (Bahramian and Degenaar, 2023). The light curves of such outbursts often follow a Fast-Rise, Exponential-Decay (FRED) profile, although variations and more complex morphologies are observed (Güngör et al., 2014).

Among neutron-star LMXBs, a particularly important subclass is the Accreting Millisecond X-ray Pulsars (AMXPs). These systems exhibit coherent millisecond pulsations in their X-ray emission, produced by magnetically channelled accretion onto the magnetic poles of the rapidly rotating neutron star. The detection of such pulsations provides direct evidence of the long-predicted link between LMXBs and millisecond radio pulsars, supporting the "recycling" scenario in which prolonged accretion spins up an old neutron star to millisecond periods (Wijnands and van der Klis, 1998).

A subset of these sources, known as *intermittent AMXPs*, show pulsations that appear and disappear over timescales ranging from hours to days, even within a single outburst. This intermittent behavior is believed to result from fluctuations in the magnetospheric configuration or the geometry of the accretion flow near the stellar surface, which can hinder or obscure the detectability of pulsations (Patruno and Watts, 2021; Bult et al.,

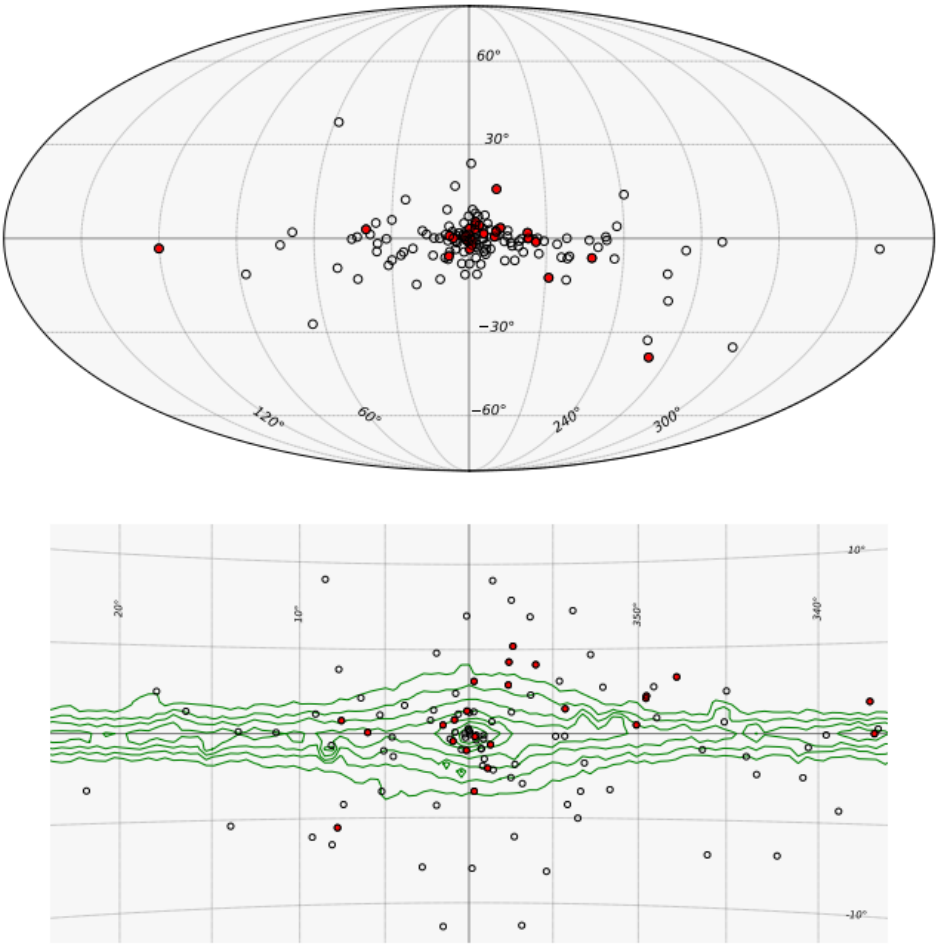

Figure 2.1: Spatial distribution of Galactic LMXBs **Top:** All-sky Aitoff projection in Galactic coordinates showing the concentration of LMXBs (red and black points) toward the Galactic plane and bulge. **Bottom:** Zoomed view of the central region with green contours tracing the stellar mass density model of the Milky Way. Most LMXBs are located within a few degrees of the Galactic plane, with a pronounced clustering in the bulge region. Figure adapted from Sazonov et al. (2020).

2018). Intermittent AMXPs serve as a link between persistent AMXPs and non-pulsating LMXBs, providing important information about how magnetic fields, accretion flows, and the evolution of neutron star spin are connected.

2.3 Spectral States in LMXBs

The X-ray spectra and variable features of LMXBs exhibit various states that signify changes in the geometry, temperature, and optical depth of the accretion flow. These spectral states are directly correlated with the mass accretion rate and the configuration of the accretion disk, corona, and boundary layer surrounding the compact object (Hasinger and van der Klis, 1989; van der Klis, 2006; Done et al., 2007; Bult et al., 2018; Putha et al., 2024).

2.3.1 Overview of Spectral States

The two principal spectral states in LMXBs are the *hard state* and the *soft state*, with additional *intermediate* or *transitional* states marking the evolution between them. These states are characterized by distinct energy spectra and timing behaviors observable in X-ray Power Density Spectra (PDS), CCDs, and HIDs.

Hard State: In the hard or island state, the X-ray spectrum is dominated by a hard, non-thermal component with a power-law $\Gamma \sim 1.5$-2.0, extending up to ~ 100 keV (Done et al., 2007; Bult et al., 2018). This emission arises from inverse Compton scattering of soft seed photons by high-energy electrons in a hot, optically thin corona. The accretion disk is likely truncated at a larger radius, with an inner hot, radiatively inefficient flow replacing the inner disk. Timing analysis reveals strong aperiodic variability with fractional rms amplitudes of 20-40%, and broad noise components in the PDS, sometimes accompanied by low-frequency quasi-periodic oscillations (QPOs) at 0.1-30 Hz (van der Klis, 2006; Belloni, 2010).

Intermediate State: During the transition from the hard to soft state, the power-law component softens ($\Gamma \sim 2.0$-2.4), while a thermal component from the disk begins to emerge as the inner radius of the disk moves inward. The total luminosity increases and variability decreases (rms $\sim$10-20%). These transitions occur over timescales of days and are associated with major changes in the disk-corona geometry and the launching or quenching of relativistic jets (Fender et al., 2004; Bult et al., 2018).

Soft State: In the soft or banana state, the spectrum is dominated by a multi-temperature accretion disk blackbody with inner disk temperatures of $kT_{\rm in} \sim 0.5$-2 keV. The Comp-

tonized component becomes weak and steep ($\Gamma \sim 2.5$-3.0), indicating a cooler, optically thicker corona. The boundary layer on the neutron-star surface contributes an additional quasi-thermal component at $\sim$ 2-3 keV. The variability amplitude decreases significantly (rms $\lesssim 5\%$), and the PDS is dominated by weak, broad features or high-frequency QPOs up to the kilohertz range (Hasinger and van der Klis, 1989; van der Klis, 2006; Putha et al., 2024).

2.3.2 Spectral Evolution and Diagnostics

The progression through these spectral states is commonly visualized using CCD and HID. The source follows a hysteresis pattern in the HID: during an outburst, the hard-to-soft transition occurs at higher luminosity than the reverse soft-to-hard transition during the decay (Maccarone and Coppi, 2003; Güngör et al., 2014; Putha et al., 2024). This hysteresis reflects differences in the efficiency of disk evaporation and condensation processes between the rise and decay phases.

2.3.3 Physical Interpretation

Spectral state transitions in LMXBs correspond to changes in the structure and dominance of the accretion components:

1. **Disk Geometry:** In the hard state, the accretion disk is truncated, and the inner region is occupied by a geometrically thick, optically thin flow (possibly an advection-dominated accretion flow; ADAF). In the soft state, the disk extends inward to the innermost stable circular orbit (ISCO).

2. **Corona and Boundary Layer:** The corona dominates the emission in the hard state but weakens in the soft state. For neutron-star systems, an additional boundary-layer component appears due to thermal emission from the stellar surface where accreting material impacts.

3. **Magnetosphere and Jets:** In some sources, including Aql X-1, the magnetosphere may truncate the inner disk and affect the spectral hardness. Radio observations indicate that steady jets are associated with the hard state, while they are quenched in the soft state (Fender et al., 2004; Migliari and Fender, 2006).

2.4 Color-Color Diagrams and Hardness-Intensity Diagrams

CCDs and HIDs are widely used, model-independent tools to study the spectral evolution of LMXBs. Both diagnostics are constructed from X-ray count rates in different energy bands, making them especially powerful for tracking spectral state transitions across outbursts.

A CCD is produced by plotting one hardness ratio against another, where a hardness ratio is defined as the ratio of count rates in two different energy bands. Neutron-star LMXBs trace distinct tracks in CCDs that reflect their accretion states and variability. Atoll sources, such as Aql X-1, display a "C-shaped" or "banana-island" track, while Z sources trace "Z-shaped" patterns and remain persistently bright near the Eddington luminosity (Bahramian and Degenaar, 2023; Hasinger and van der Klis, 1989). The morphology of CCDs therefore serves as a clear diagnostic of the physical state of the system.

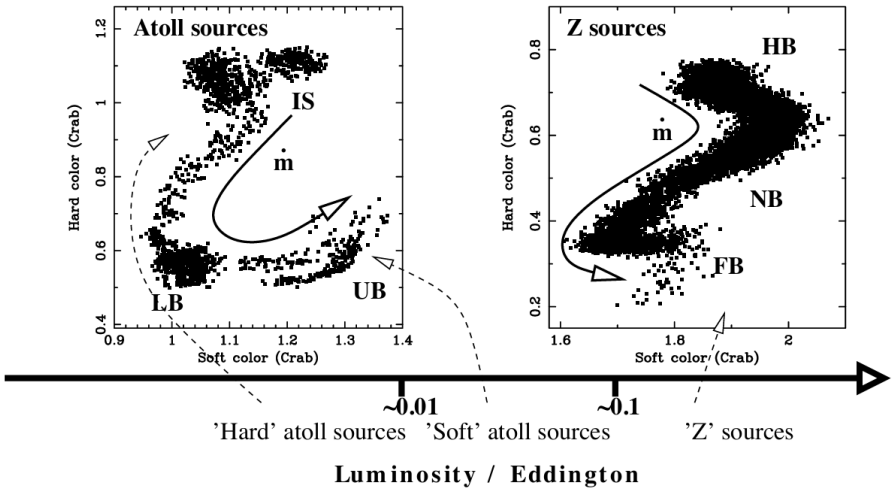

Figure 2.2: CCDs of atoll and Z sources from Hasinger and van der Klis (1989). The left panel shows the "C-shaped" track of atoll sources, while the right panel shows Z sources tracing a "Z-shaped" path through the horizontal (HB), normal (NB), and flaring (FB) branches corresponding to increasing mass accretion rates ($\dot{M}$). The bottom axis indicates the typical luminosity range of these sources in units of the Eddington luminosity ($L/L_{\rm Edd}$), linking atoll and Z sources into a unified accretion sequence.

HIDs complement CCDs by plotting a hardness ratio against total source intensity. For systems like Aql X-1, HIDs reveal a characteristic loop that traces the hard, intermediate, and soft states as the accretion rate evolves during outbursts. These diagrams provide an intuitive view of spectral evolution and allow the classification of transient behavior across multiple outbursts (Güngör et al., 2014; Putha et al., 2024).

2.5 Aquila X-1

Aquila X-1 (Aql X-1) is a transient neutron star LMXB and one of the most frequently outbursting systems of its kind. It is located in the constellation Aquila at an estimated distance of about 5 kpc. The system consists of a neutron star accreting matter from a Roche lobe-filling, late-type low-mass companion in an ∼19 hr orbit (Bult et al., 2018). Aql X-1 is among the best-studied neutron-star transients because of its recurrent activity, well-monitored outbursts, and rich phenomenology spanning spectral, timing, and burst behaviors.

2.5.1 Neutron Star Characteristics and Observational History

The neutron star in Aql X-1 exhibits several distinctive characteristics that have been established through decades of X-ray observations. Its spin frequency, inferred from coherent oscillations during thermonuclear (type-I) X-ray bursts, is approximately 550 Hz, making it one of the fastest known accreting neutron stars. These burst oscillations, first detected with the *Rossi X-ray Timing Explorer (RXTE)*, are interpreted as brightness asymmetries on the neutron star surface caused by nuclear burning spreading across the star during type-I bursts. The oscillation frequency remains nearly constant across multiple bursts, providing robust evidence for the stellar spin rate and confirming the presence of a rapidly rotating neutron star.

In addition to burst oscillations, Aql X-1 occasionally exhibits *intermittent accretion-powered pulsations*, detected during some outbursts but absent in others. These pulsations appear sporadically and last for only a few hundred seconds at a time, with an amplitude of ∼1-2%, as observed in RXTE and later with NICER. The intermittent nature of these pulsations suggests that the magnetic field is relatively weak ($B \sim 10^8$–10^9 G), allowing the accretion flow to reach close to the stellar surface without producing persistent pulsations. Possible explanations include transient channelling of the accretion flow, partial obscuration by scattering material near the magnetosphere, or changes in the magnetic field geometry (Bult et al., 2018). This behavior places Aql X-1 among the class of Accreting Millisecond X-ray Pulsars (AMXPs), bridging the gap between persistently pulsating systems and non-pulsating neutron-star LMXBs.

Aql X-1 has been extensively observed across multiple X-ray missions, including *EXOSAT*[1], *RXTE*, *Swift*[2], *MAXI* subsection 2.6.1, and more recently, *NICER* subsection 2.6.2. These long-term campaigns have enabled detailed studies of its outburst recurrence and spectral evolution. The system usually has outbursts every few hundred

[1]European X-ray Observatory Satellite
[2]Neil Gehrels *Swift* Observatory

days, with recurrence intervals ranging from ∼125 to 300 days and an average cycle of ∼250 days (Bult et al., 2018). Each outburst exhibits a rise in X-ray luminosity by several orders of magnitude, followed by an exponential decay back to quiescence, consistent with the thermal-viscous disk instability model.

2.5.2 Outburst Behavior and Spectral States

The outbursts of Aql X-1 display a wide range of profiles and peak luminosities, from dim events reaching only ∼5% of the Eddington limit to bright episodes exceeding 30% of $L_{\rm Edd}$ (Bult et al., 2018). During these outbursts, the source transitions through the canonical spectral states characteristic of atoll-type LMXBs. At low luminosities, it occupies the extreme island (hard) state, where emission is dominated by Comptonized radiation from a hot corona and strong broad-band noise is present. As the luminosity increases, the source moves into softer states dominated by thermal emission from the accretion disk and boundary layer, while variability decreases (Bult et al., 2018; Putha et al., 2024).

Aql X-1 is also classified as a soft X-ray transient (SXT). In quiescence, its X-ray luminosity drops to $L_X \approx 10^{33}$ erg s^{-1}, rising to $\sim 10^{37}$ erg s^{-1} during outbursts due to enhanced accretion rates in the disk (Güngör et al., 2014). These transitions are understood within the framework of the disk instability model (DIM), where thermal-viscous instabilities in the disk trigger episodic mass accretion onto the neutron star.

Using extensive monitoring with *RXTE*/ASM and *MAXI*, Güngör et al. (2014) identified three distinct categories of Aql X-1 outbursts: *long-high*, *medium-low*, and *short-low*. The long-high type lasts ∼50-60 days and reaches the highest luminosities; medium-low outbursts last 40-50 days with moderate peak fluxes; and short-low events span ∼20 days with lower intensities. Despite differences in duration and brightness, all types show similar spectral evolution, with outer disk irradiation being the dominant factor shaping the outburst profiles.

2.5.3 Recent NICER Observations

Recent observations with NICER have provided high-throughput, soft X-ray coverage of Aql X-1, enabling precise studies of its spectral evolution during the 2019 and 2020 outbursts (Putha et al., 2024). The spectra are well described by a combination of thermal emission from a multi-temperature accretion disk and a Comptonized component, with inner disk temperatures around 0.6-0.8 keV and coronal electron temperatures of a few keV. The detection of Fe Kα emission indicates reprocessing of hard photons in the disk, while absorption features point to additional local material beyond the Galactic interstellar medium. These results highlight Aql X-1's role as a benchmark system for

understanding accretion dynamics, magnetic field interactions, and spectral state transitions in neutron-star LMXBs.

2.6 Instruments and Observational Coverage

2.6.1 MAXI: All-Sky Monitor

MAXI's ability to scan the entire sky once every 92 minutes enables it to serve as an early-warning system for transient events such as outbursts in low-mass X-ray binaries. Because Aql X-1 undergoes irregular but recurrent outbursts, continuous coverage is essential for detecting the precise onset of activity. The near real-time data processing pipeline of MAXI provides light curves and flux alerts that are publicly distributed within hours of observation. This makes it possible to identify even modest increases in soft X-ray flux and to distinguish them from background fluctuations, ensuring rapid recognition of the beginning of an outburst.

Once such an increase is detected, astronomers can initiate Target of Opportunity (ToO) observations with more sensitive, pointed instruments such as NICER, HXMT[3], or NuSTAR[4]. These observatories have narrower fields of view and cannot monitor the sky continuously, but they provide far greater spectral and timing resolution. The synergy between MAXI and these pointed missions is therefore critical: MAXI detects the outburst and provides global context, while the follow-up observations yield detailed measurements of spectral parameters, variability properties, and accretion dynamics. In this way, MAXI acts as the primary trigger that bridges the gap between wide-field monitoring and high-precision studies of transient accreting systems.

2.6.2 NICER: Soft X-ray Timing Instrument

The Neutron Star Interior Composition Explorer (NICER) is a modern X-ray timing and spectroscopy instrument mounted on the International Space Station (ISS) since June 2017. NICER was specifically designed to investigate the interior composition of neutron stars by measuring their radii and masses with high precision, thereby constraining the equation of state of ultra-dense matter. Its instrumentation consists of 56 co-aligned X-ray concentrators coupled to silicon drift detectors, yielding a peak effective collecting area of approximately 1900 cm^2 at 1.5 keV.

[3]Hard X-ray Modulation Telescope (HXMT): China's first X-ray astronomy satellite, designed to study celestial sources in the hard X-ray band (1-250 keV).

[4]Nuclear Spectroscopic Telescope Array (NuSTAR): NASA's focusing hard X-ray telescope operating in the 3-79 keV range, providing high sensitivity and angular resolution.

NICER operates in the 0.2–12 keV soft X-ray band with excellent spectral resolution (85 eV at 1 keV) and unmatched timing resolution of about 100 nanoseconds. This combination of capabilities enables NICER to perform simultaneous high-resolution spectral and temporal studies of compact objects. Owing to its location on the ISS, NICER can flexibly monitor transient and variable sources with dense temporal coverage, making it well suited for studying full outburst cycles of LMXBs such as Aql X-1. Data products generated by NICER include event files, light curves, and spectra, which are distributed through HEASARC and analyzed using the HEASoft software suite. The unique synergy of large collecting area, sensitivity in the soft X-ray regime, and precise timing capabilities makes NICER an indispensable tool for exploring accretion dynamics, thermonuclear bursts, and state transitions in neutron star X-ray binaries.

Chapter 3

Data and Methods

3.1 Observations

The dataset analyzed in this study was obtained with the NICER during the 2023 (25 June 2023 to 13 September 2023) and 2024 (20 September 2024 to 13 November 2024) outbursts of Aql X-1. A total of 81 NICER observations covering the complete rise, peak, and decay phases of both the 2023 and 2024 outbursts were initially obtained. After standard screening GTIs (section 3.2), 79 high-quality observations were retained for analysis; two ObservationIDs (ObsIDs) were excluded due to elevated undershoot rates that did not meet the data-quality thresholds. The final dataset provides sufficient temporal coverage to track the spectral evolution continuously and to identify transitions between accretion states.

The observations were chosen based on several quality criteria: stable pointing and attitude solutions, absence of contamination from enhanced background or optical loading, and exclusion of intervals affected by the South Atlantic Anomaly (SAA). Only observations with adequate exposure times to ensure statistically meaningful spectra in the 0.6-10 keV band were included. This extensive coverage enabled the examination of the spectral-timing evolution across both outbursts and facilitated the identification of state transitions between the canonical atoll source branches (island to banana).

3.2 Data Reduction

Data from all NICER observations were processed using the HEASoft[5] software suite software suite (version 6.34) with the NICERDAS[6] pipeline and the latest calibration database (CALDB). Standard screening and calibration procedures were applied to obtain clean, calibrated Level 2 event files suitable for spectral and timing analysis.

Level 2 Processing

Raw event files were processed through the `nicerl2` task to produce calibrated data. The main screening steps included:

- **Pointing and attitude:** Time intervals with unstable pointing or large attitude offsets were excluded. The option `mpu_strict_filter=YES` was used to remove brief periods of noisy detector activity. There were a lot of quality checks done during data screening.
- **SAA and background:** Data obtained during the passing of NICER through the South Atlantic Anomaly (SAA) or when the geomagnetic cutoff rigidity was low were eliminated to reduce contamination from high-energy particles.
- **Optical contamination:** Time intervals affected by bright-Earth illumination or optical loading were excluded by applying limits on the Earth limb and bright-Earth angles.
- **Detector health:** Any detectors flagged as inactive or unstable in the calibration files were removed from use, and gain corrections were applied to maintain consistent energy calibration across all modules.

After these steps, the processed data yielded clean Level 2 event files (`*.evt`) and corresponding Good Time Intervals (GTIs), representing periods of reliable and high-quality observations.

Good Time Intervals (GTIs)

GTIs were generated by removing time periods with high background, excessive overshoot or undershoot rates, and brief pointing drifts. The `mgtime` task was used to combine all screening conditions, retaining only intervals that met every quality criterion. These GTIs were used in all subsequent spectral and timing analyses.

[5]High Energy Astrophysics Software (HEASoft): the NASA-developed suite for X-ray and gamma-ray data reduction and analysis.

[6]NICER Data Analysis Software (NICERDAS): the NICER-specific data processing pipeline within HEASoft.

Deadtime and Exposure Corrections

NICER observations can be affected by detector deadtime, especially at high count rates. Livetime corrections applied by the NICER pipeline were used to account for this effect.

3.3 Spectral Extraction

Spectra were extracted in the 0.6-10 keV energy range, where the NICER response is well calibrated and background contamination is minimal. Data below 0.6 keV were excluded due to calibration uncertainties, and channels above 10 keV were omitted because of reduced sensitivity and higher background levels.

Source spectra were produced for each observation using the `nicerl3-spect` task. This process generated photon energy distributions and attached the appropriate response files: the Redistribution Matrix File (RMF) and the Ancillary Response File (ARF). The response versions corresponding to the correct gain epoch were verified to ensure consistency across all observations.

Background Modeling

Background spectra were created using NICER's standard background estimation tools. The SCORPEON model was adopted as the default, as it accounts for particle, cosmic, and optical background components based on housekeeping data such as overshoot rates, geomagnetic conditions, and pointing direction. For comparison, additional background spectra were generated using the 3C50 model. Differences between the two models were used to estimate systematic uncertainties, especially at higher energies where background contributions are more crucial.

Spectral Grouping and Statistics

Each spectrum was grouped to contain a minimum of 25 counts per bin using `ftgrouppha`, ensuring the validity of χ^2 statistics. For lower-count spectra, C-statistics were used as a consistency check, although χ^2 minimization was adopted for all final fits.

3.4 Spectral Modeling

Spectral fitting was carried out in XSPEC[7] (version 12.14.1) using a range of physically motivated models to determine the best representation of the observed X-ray spectra. Several combinations were initially tested, including `tbabs*(bbody+powerlaw)`, `tbabs*(diskbb+bbodyrad)`, `tbabs*(diskbb+nthcomp)`, and `tbabs*(diskbb+powerlaw)`. These models use different physical elements, like a blackbody to show emission from the neutron star's surface or boundary layer, a multicolor disk blackbody (diskbb) to show the accretion disk, and power-law or Comptonization components to show high-energy emission from inverse Compton scattering in a corona.

Despite these trials, none of the above models provided statistically acceptable fits, as indicated by their relatively poor χ^2 values and structured residuals. Consequently, these models were excluded from further consideration.

The best representation of the spectra was achieved using the `tbabs*nthcomp` model. This model combines the effects of interstellar absorption (`tbabs`) with thermal Comptonization (`nthcomp`), which describes the upscattering of soft seed photons by a population of hot electrons in a corona surrounding the compact object. The `nthcomp` model is particularly well suited for neutron star LMXBs, as it allows for the characterization of the Comptonizing plasma's temperature and optical depth, as well as the nature of the seed photons, which can originate from either the neutron star surface or the accretion disk. This configuration provided the most physically consistent and statistically robust fits to the observed spectra.

Model Parameters

The absorption component `tbabs` was used to describe interstellar photoelectric absorption, parameterized by the equivalent hydrogen column density ($N_{\rm H}$) in units of 10^{22} cm^{-2}. The photoionization cross-sections of Verner et al. (1996) and the abundances of Wilms et al. (2000) were adopted.

The thermal Comptonization component `nthcomp` included the following parameters:

- (Γ), defining the slope of the power-law continuum;
- ($kT_{\rm e}$), representing the temperature of the Comptonizing plasma;

[7] XSPEC is an X-ray spectral fitting package developed and maintained by NASA's High Energy Astrophysics Science Archive Research Center (HEASARC). It provides a flexible environment for modeling and analyzing astronomical X-ray spectra.

- ($kT_{\rm bb}$); representing the seed photon temperature
- Normalization, scaling the overall flux of the Comptonized emission.

3.5 CCD Construction

CCDs were created to study the spectral evolution of Aql X-1 without relying on model fitting. The soft color was defined as the ratio of counts in the 1.8-3.5 keV to 0.5-1.8 keV bands, and the hard color as the ratio of counts in the 5.2-6.8 keV to 3.5-5.2 keV bands. These ranges were selected to represent different parts of the spectrum while avoiding strong instrumental edges.

Band-limited light curves were generated using `nicerl3-lc`, and average count rates were calculated over the GTIs for each observation. Background count rates were subtracted, and errors were propagated using standard uncertainty formulas. Observations with very low count rates or poor background estimates were excluded.

The CCDs revealed two main spectral branches: the hard, low-intensity island state and the soft, high-intensity banana branch. Transitions between these states were identified from the trajectories traced by the data points in color-color space.

3.6 Timing and Statistical Analysis

Light curves were produced in the 0.6-10 keV range using a time resolution of 0.001 s. Deadtime corrections and GTIs were applied consistently with those used for spectral analysis. Fractional root-mean-square (rms) variability was measured to quantify short-term flux changes.

Fractional RMS Variability

The fractional rms amplitude was obtained from Fourier power spectra computed over data segments of 16-64 s. The averaged power spectra were corrected for Poisson noise, and the integrated power in the 0.1-64 Hz range provided the fractional rms variability. Errors were estimated from the scatter among individual segment powers, with corrections applied for any deadtime effects.

Statistical Confidence and Systematic Uncertainties

Spectral fits were evaluated using χ^2 minimization. Acceptable fits were indicated by reduced χ^2 values near unity. Parameter uncertainties were quoted at the 90% confidence

level. When parameters such as kT_e were poorly constrained within the NICER bandpass, large error ranges were reported or the parameter was fixed to a representative value for stability.

The fits were visually inspected to ensure that calibration or background effects did not significantly affect the results. Consistent procedures were followed across both outbursts to maintain reliability and comparability of all measurements.

Millisecond Pulsation Search

A detailed search for coherent millisecond pulsations was performed to investigate accretion-powered signals from the neutron star in Aql X-1. The NICER event files were processed to extract photon arrival times in the 0.6-10 keV energy range and converted to text format for timing analysis. These arrival times were analyzed using the Z_n^2 statistic (Buccheri et al., 1983), implemented through the `Stingray` timing package.

The search was centered on the known spin frequency of Aql X-1 (555 Hz) and spanned a range of 535-575 Hz with a frequency resolution of 0.1 Hz. The Z_n^2 statistic was evaluated at each trial frequency using two harmonics ($n = 2$) to capture possible non-sinusoidal pulse profiles. To estimate the statistical significance of candidate peaks, 500 bootstrap realizations were generated to construct a null-hypothesis distribution of Z_n^2 values. The observed maximum Z_n^2 was then compared against this distribution to derive confidence thresholds (1σ, 2σ, and 3σ) and the corresponding p-values.

No statistically significant or persistent pulsations were detected during either the 2023 or 2024 outburst. The non-detection implies that any coherent pulsations, if present, were below the sensitivity limits of this analysis, consistent with previous reports of transient, low-amplitude pulsations in Aql X-1 (Casella et al., 2008; Bult and van der Klis, 2015; Bult et al., 2018).

Software and Model References

- HEASoft and NICERDAS documentation (NASA/GSFC) (NASA/GSFC, 2024).
- XSPEC (Arnaud, 1996).
- `tbabs` (Wilms et al., 2000).
- `nthcomp` (Zdziarski et al., 1996; Życki et al., 1999).

- NICER instrument (Gendreau et al., 2016).
- NICER background models (NICER Team, 2024).
- `Stingray` (Huppenkothen et al., 2019).

Chapter 4

Results

4.1 Light Curves

The NICER observations of Aql X-1 during the 2023 and 2024 outbursts provide well-sampled X-ray light curves covering the rise, peak, and decay phases of both events. The light curves, extracted in the 0.6-10 keV band, are shown in Figures 4.1 and 4.2. To enable a direct comparison with the MAXI monitoring data (2-20 keV), the NICER count rates were empirically mapped onto the MAXI count-rate scale. This was achieved by rebinning the NICER light curve to a daily cadence and performing a least-squares linear fit of the form

$$R_{\mathrm{MAXI}} = a \times R_{\mathrm{NICER}} + b,$$

using the overlapping intervals between the two instruments. The resulting transformation converts the NICER light curve into MAXI-equivalent units, allowing both datasets to be displayed on a common y-axis for comparison (see Figure 4.3). This mapping is empirical and intended for relative comparison of flux evolution rather than absolute calibration, since the two instruments have different energy responses and effective areas. While both outbursts exhibit the overall pattern characteristic of transient neutron-star LMXBs, their detailed profiles differ in duration, peak flux, and decay morphology.

4.1.1 2023 Outburst

The 2023 outburst (Figure 4.1) began around MJD 60150 at very low flux levels. The source exhibited a steep rise, reaching a peak flux of $\sim$3.2 ph s^{-1} cm^{-2} by MJD 60160. This rapid increase over $\sim$10 days is consistent with a thermal-viscous instability in the accretion disk, where accumulated material is suddenly accreted onto the neutron star.

A brief plateau was observed between Mean Julian Days(MJD) 60160-60165, after which the flux decayed smoothly until MJD 60200. The decay followed an exponential-like trend,

typical of viscous draining of the accretion disk after an instability-triggered outburst. The total duration of ∼50 days, along with the absence of rebrightenings, indicates a well-behaved, single-peaked event displaying a classic FRED profile.

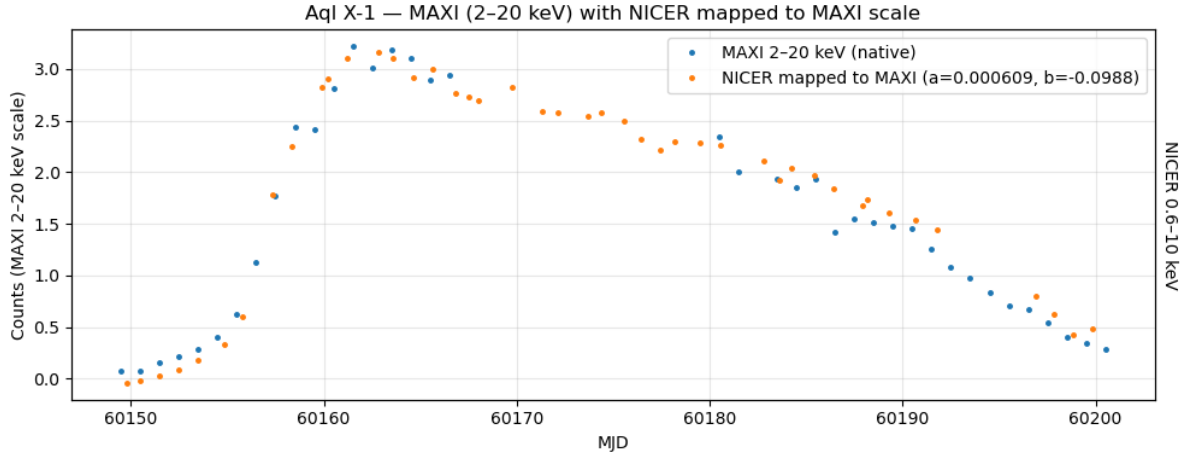

Figure 4.1: Light curve of Aql X-1 during the 2023 outburst in the 2-20 keV band (MAXI with NICER mapped to MAXI scale). The source exhibits a rapid rise to a peak of ∼3.2 ph s^{-1} cm^{-2} near MJD 60160, followed by a smooth exponential decay to quiescence by MJD 60200. The event represents a prototypical FRED-type transient outburst.

4.1.2 2024 Outburst

The 2024 outburst (Figure 4.2) began around MJD 60575 and showed a similarly rapid rise over ∼10 days, reaching a peak flux of ∼2.0 ph s^{-1} cm^{-2} by MJD 60585. Compared to 2023, the maximum flux was lower, but the source maintained a nearly constant plateau until ∼MJD 60592, suggesting a transient equilibrium between mass inflow and disk depletion.

The decay phase was shorter (∼20-25 days) and exhibited mild irregularities, including fluctuations superimposed on the general decline. This complicated decay and extended plateau phase are different from the smoother 2023 profile, potentially indicating changes in the accretion rate modulation or irradiation feedback within the disk.

4.1.3 Comparison Between the 2023 and 2024 Outbursts

A direct comparison of the two events is shown in Figure 4.3. Both outbursts display the canonical rapid-rise and slower-decay morphology typical of transient neutron-star LMXBs, but with notable quantitative and structural differences.

The 2023 outburst reached a higher luminosity, lasted longer (∼50 days), and exhibited a smoother exponential decay. The event in 2024, on the other hand, was shorter and less bright, with a clear plateau and little change during the decay. These distinctions may reflect differences in the initial disk mass reservoir, irradiation efficiency, or mass transfer

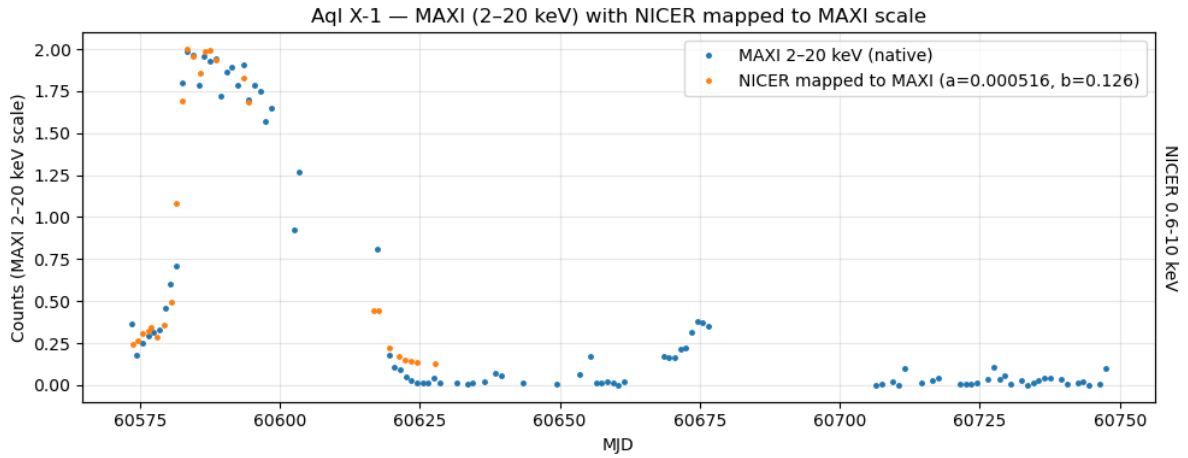

Figure 4.2: Light curve of Aql X-1 during the 2024 outburst in the 2-20 keV band (MAXI with NICER mapped to MAXI scale). The flux peaked at ∼2.0 ph s^{-1} cm^{-2} near MJD 60585 and remained approximately constant until ∼MJD 60592 before declining with short-term fluctuations. The 2024 event was shorter and less luminous than the 2023 outburst.

rate from the companion star. Such variations between successive outbursts of the same system are common among recurrent transients like Aql X-1 and offer valuable clues to the disk-accretion cycle and state transition dynamics.

4.2 Spectral Fitting

All spectra were modeled in the 0.6-10 keV range using the absorbed thermal Comptonization model `tbabs*nthcomp`. The `tbabs` component accounts for interstellar and possible local absorption, while `nthcomp` describes up-scattering of soft seed photons in a hot electron plasma. The free parameters of the model are the hydrogen column density ($N_{\rm H}$), (Γ), (kT_e), ($kT_{\rm bb}$), and normalization. The seed photons were assumed to originate from a disc geometry (`inp_type = 1`).

The fits were initialized with typical starting values of $N_{\rm H} = 0.4 \times 10^{22}\,{\rm cm}^{-2}$, $\Gamma = 2.0$, $kT_e = 3$ keV, $kT_{\rm bb} = 0.35$ keV, and `inp_type = 1`. These values ensured convergence across the full data set. The unfolded spectrum shown in Fig. 4.4 shows the quality of the fits: the model reproduces the data well with residuals randomly scattered around zero. Reduced χ^2 values consistently range from 1.0 and 1.5, signifying that the adopted model adequately describes the NICER spectra without the need for additional continuum or line components.

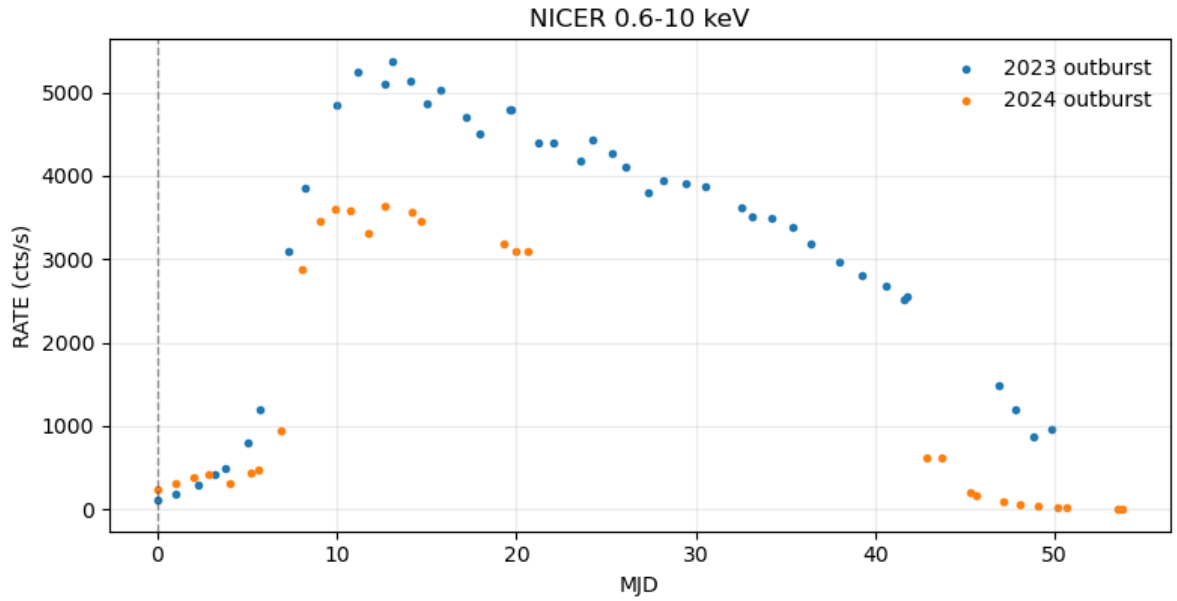

Figure 4.3: Comparison of NICER 0.6-10 keV light curves of Aql X-1 during the 2023 and 2024 outbursts. The 2023 event (blue) reached a higher peak and lasted longer, while the 2024 event (orange) was fainter and more structured. Both exhibit the characteristic FRED morphology of transient LMXB outbursts.

4.3 Spectral Parameter Evolution

Figures 4.5 and 4.6 present the evolution of the spectral parameters throughout the 2023 and 2024 NICER-observed outbursts of Aql X-1. Each panel shows the X-ray light curve followed by the temporal variation of $N_{\rm H}$, Γ, $kT_{\rm e}$, $kT_{\rm bb}$, and the unabsorbed flux.

During both outbursts, the absorption column density $N_{\rm H}$ remained relatively stable at (3-4.5) $\times$ 10^{21} cm^{-2}, consistent with the Galactic foreground value toward the source, suggesting no significant intrinsic absorption.

In the 2023 outburst, the light curve exhibits a rapid rise followed by a smooth decay. At the onset, the spectrum is relatively soft with $\Gamma \approx$ 2.1-2.3 and $kT_{\rm e} \sim$ 4-6 keV, indicating a moderately Comptonized state. As the flux rises, Γ decreases to $\sim$ 1.7-1.8, showing that the spectrum becomes harder toward the outburst peak. This hardening suggests that the Comptonized component strengthened relative to the soft emission, possibly due to increased coronal heating or a higher optical depth. During the decay phase, Γ remains nearly constant within the range 1.7-1.9, while the $kT_{\rm e}$ stays around a few keV with little systematic variation. The $kT_{\rm bb}$ remains roughly stable at $\sim$ 0.5-0.7 keV, consistent with a steady inner disk contribution. The unabsorbed flux follows the general light curve, with a peak about MJD 60160 and then a smooth drop, reflecting the gradual depletion of the accretion disk as the outburst subsides.

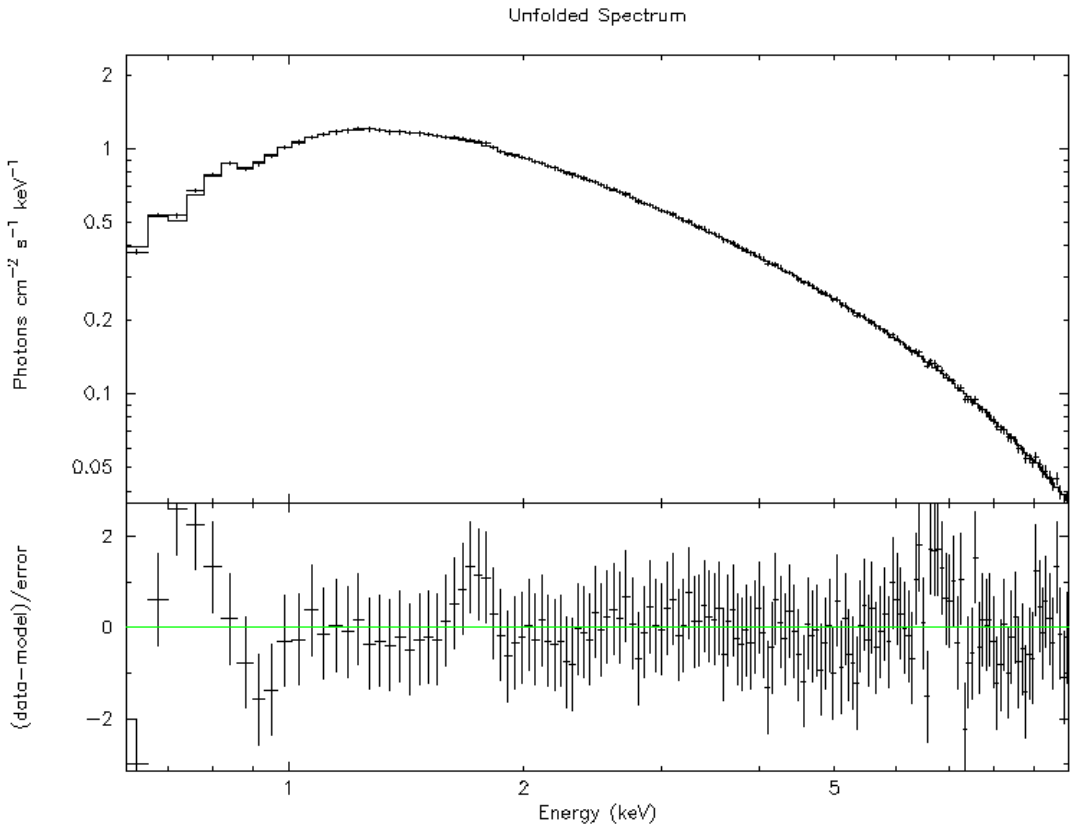

Figure 4.4: Unfolded spectrum fitted with `tbabs*nthcomp`. The upper panel shows the best-fit model and data in photons cm^{-2} s^{-1} keV^{-1}, and the lower panel shows residuals in units of (data − model)/error. The fit is statistically acceptable with reduced $\chi^2 \approx 1$–1.5.

The 2024 outburst shows a shorter and more impulsive evolution. The flux rises steeply and reaches its maximum earlier than in 2023, followed by a relatively fast decay. Spectrally, it begins in a harder state ($\Gamma \sim 1.6$-1.8) and remains less softened near the peak, with higher $kT_{\rm e}$ values (up to several keV) indicating a hotter and more dominant Comptonizing corona. The moderate increase in Γ and decrease in $kT_{\rm e}$ toward the decay phase suggest a brief softening episode, though less pronounced than in 2023. The $kT_{\rm bb}$ evolution remains confined between 0.4-0.8 keV, again consistent with thermal emission from the inner disk.

Overall, the 2024 event was both harder and shorter in duration, pointing to a relatively higher coronal contribution and possibly a truncated accretion disk compared to 2023. In both cases, the unabsorbed flux tracks the overall outburst morphology, peaking near the spectral softening phases.

Some data points appear without visible error bars, particularly in $kT_{\rm e}$. These correspond to spectra where the cutoff energy lies above NICER's 0.6-10 keV bandpass, rendering $kT_{\rm e}$ poorly constrained. In such cases, the model tends toward its upper limit, leading to unrealistically large formal errors. These points are not physically meaningful but represent fitting limitations rather than genuine spectral variability.

4.4 Results of the Millisecond Pulsation Search

The Z_n^2 power spectra were computed for all high-signal NICER observations in the frequency range 535-575 Hz, encompassing the known spin frequency of Aql X-1. No persistent or statistically significant periodic signals were detected during either the 2023 or 2024 outbursts. The resulting power spectra were consistent with white-noise expectations, and no peaks exceeded the 99.9% confidence threshold after correction for the number of independent frequency trials.

Representative results from two individual NICER observations (ObsIDs 6634020101 and 7050340105) are presented in Figures 4.7 and 4.8. In both cases, the Z_2^2 statistic was computed across the 535-575 Hz frequency range encompassing the known spin frequency of Aql X-1.

For ObsID 6634020101, a small power enhancement was found near 575 Hz with $Z_2^2 \approx 18$, which lies below the 1σ confidence level and is consistent with statistical noise. No other peaks within the searched frequency interval approached the 2σ or 3σ significance thresholds (approximately 30 and 42, respectively).

In ObsID 7050340105, a narrow peak was detected around 538 Hz with $Z_2^2 \approx 20$, placing it close to the 1σ confidence level but still well below the 2σ and 3σ thresholds. The remain-

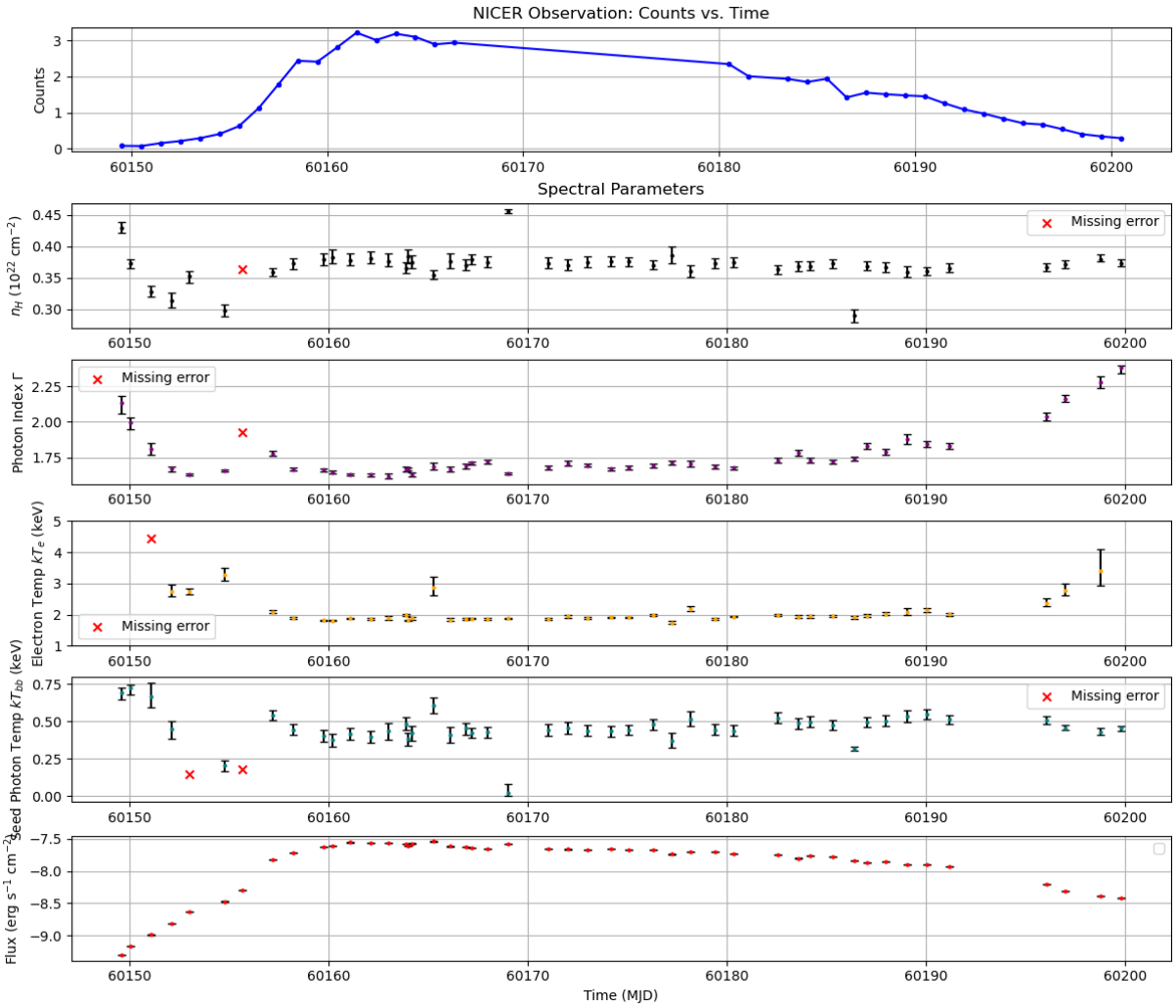

Figure 4.5: Spectral evolution of Aql X-1 during the 2023 outburst. Top panel: NICER light curve (0.6-10 keV). Lower panels: best-fit spectral parameters as a function of time - $N_{\rm H}$, Γ, $kT_{\rm e}$, and $kT_{\rm bb}$, and unabsorbed flux (0.6-10 keV). Error bars represent 1σ uncertainties.

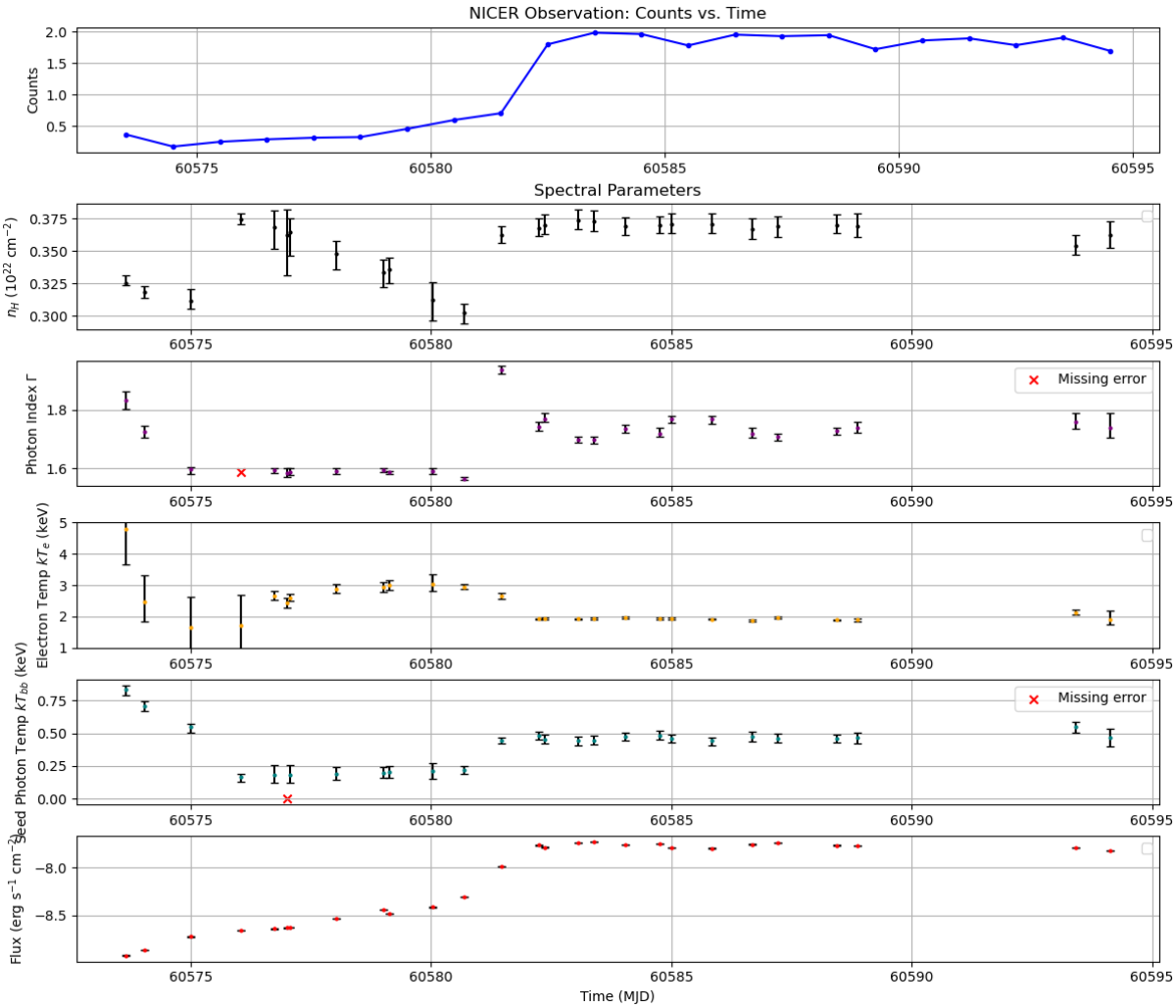

Figure 4.6: Spectral evolution of Aql X-1 during the 2024 outburst. Top panel: NICER light curve (0.6-10 keV). Lower panels: best-fit spectral parameters as a function of time - $N_{\rm H}$, Γ, $kT_{\rm e}$, $kT_{\rm bb}$, and unabsorbed flux (0.6-10 keV). Error bars represent 1σ uncertainties.

der of the power spectrum exhibits random, low-amplitude fluctuations characteristic of white noise.

As no features in either dataset exceeded the 99.9% confidence threshold or recurred consistently in other observations, the apparent excesses are interpreted as statistical fluctuations rather than genuine periodic signals. Consequently, no significant or persistent millisecond pulsations were detected in these NICER observations of Aql X-1.

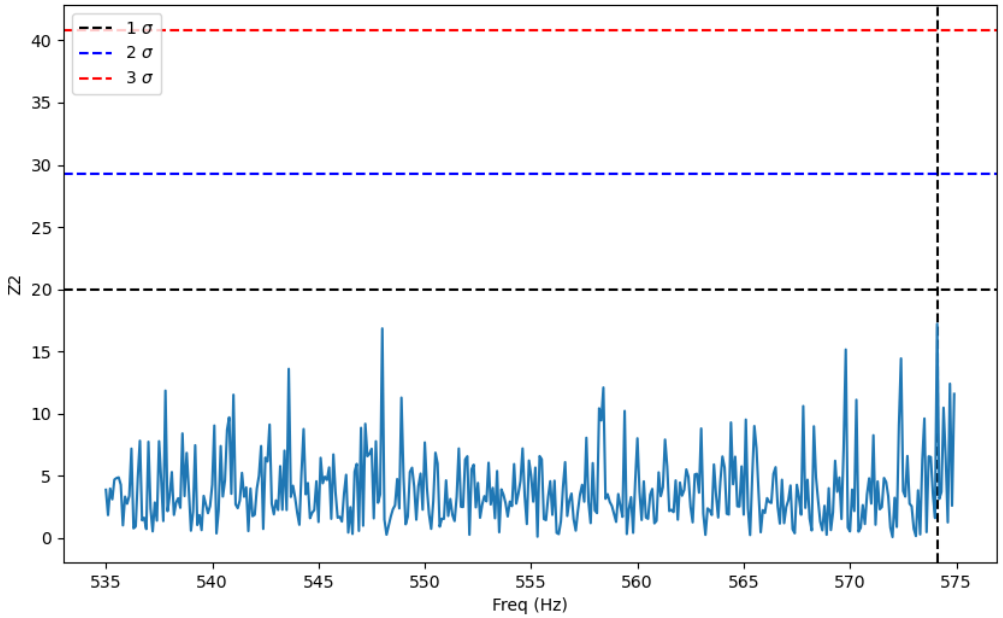

Figure 4.7: Z_2^2 statistic versus trial frequency for Aql X-1 (ObsID 6634020101). Horizontal dashed lines indicate 1σ, 2σ, and 3σ confidence thresholds derived from bootstrap simulations. No significant peaks were detected within the searched frequency range.

4.5 CCDs and HIDs

The CCDs (Figures 4.9 and 4.11) display the distribution of data points in the soft-hard color plane for the 2023 and 2024 outbursts, respectively. The data points in both graphs are spread out over a wide range of soft color values. On the other hand, the hard color only changes over a small range. The overall pattern makes a track that goes from higher hard color values to lower ones. The 2023 diagram shows that the spread is bigger at intermediate soft color values.. The 2024 diagram, on the other hand, shows a more compact distribution with more points at lower hard color values. The two diagrams therefore differ mainly in the extent of the spread and the compactness of the tracks.

The corresponding HIDs (Figures 4.10 and 4.12) show the variation of spectral hardness with total count rate. In both cases, the hard color decreases gradually as the intensity

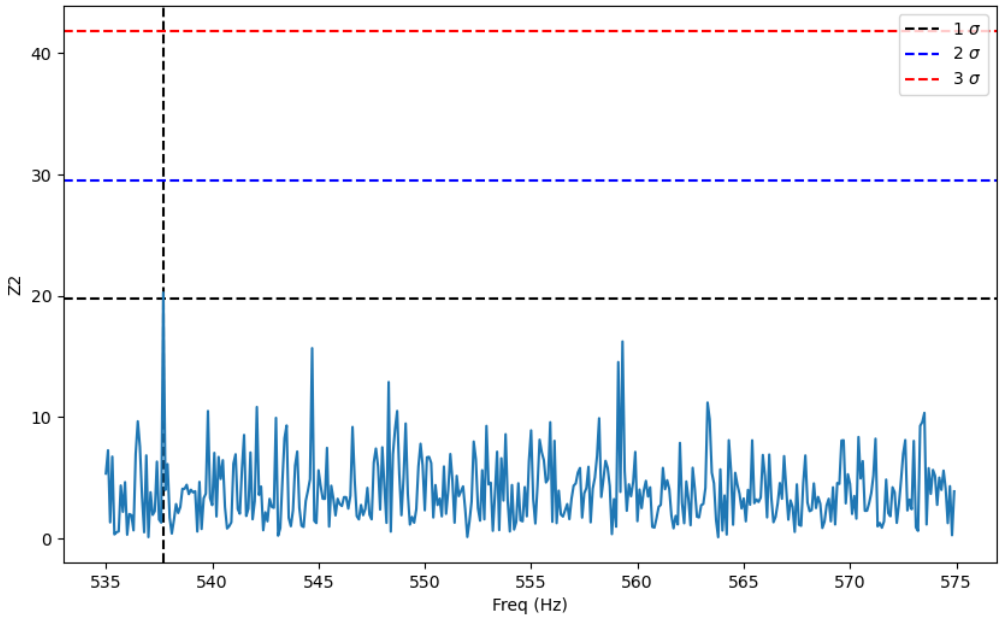

Figure 4.8: Z_2^2 statistic versus trial frequency for Aql X-1 (ObsID 7050340105). A modest feature at ∼538 Hz remains below the 2σ significance level and is consistent with noise.

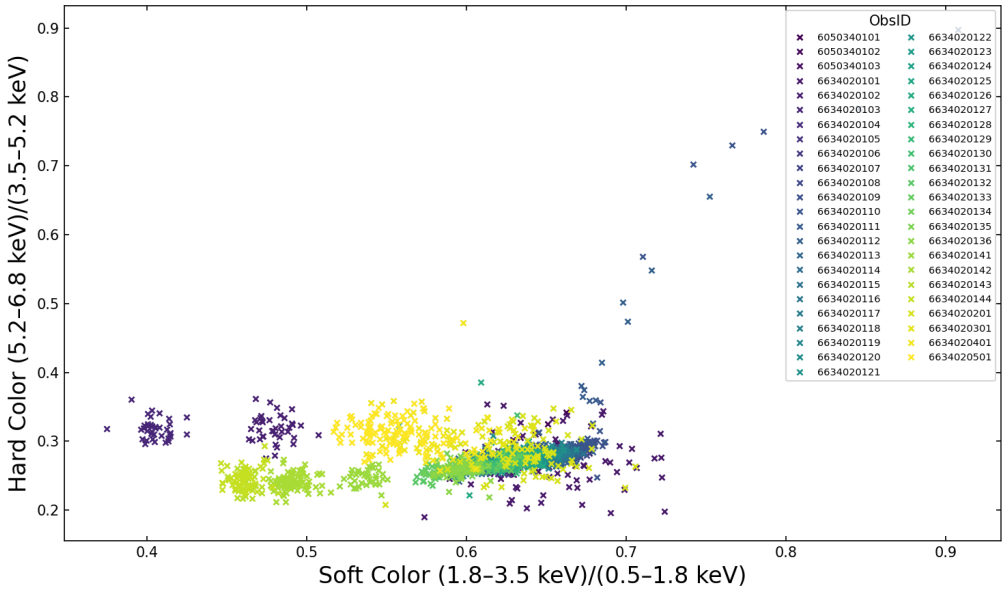

Figure 4.9: CCD of Aql X-1 during the 2023 outburst. The soft color is defined as the ratio (1.8-3.5 keV)/(0.5-1.8 keV), and the hard color as (5.2-6.8 keV)/(3.5-5.2 keV). Points are color-coded by ObsID.

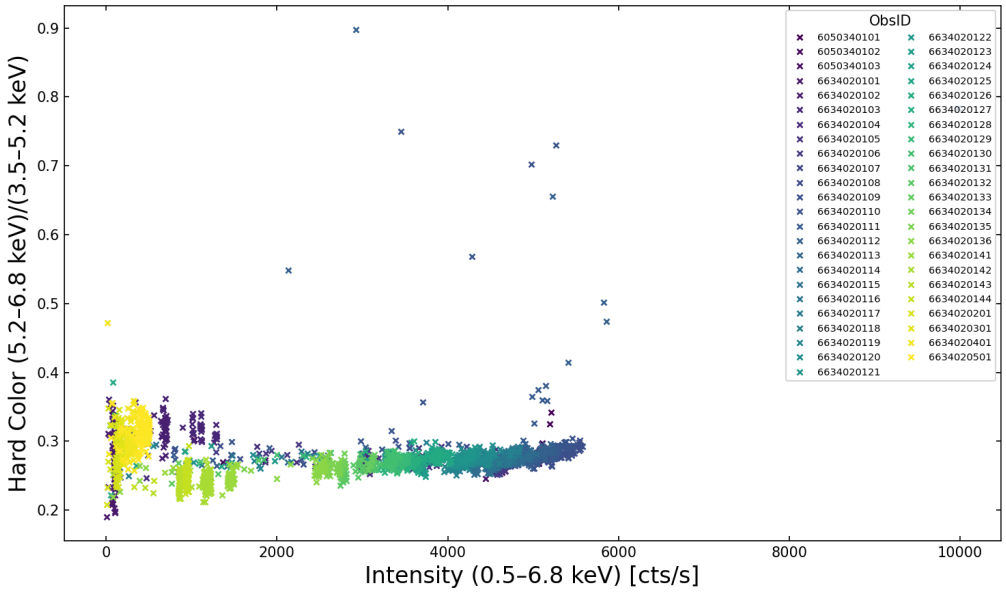

Figure 4.10: HID corresponding to the 2023 outburst. The hard color is plotted as a function of total count rate in the 0.5-6.8 keV band. Observations are color-coded by ObsID.

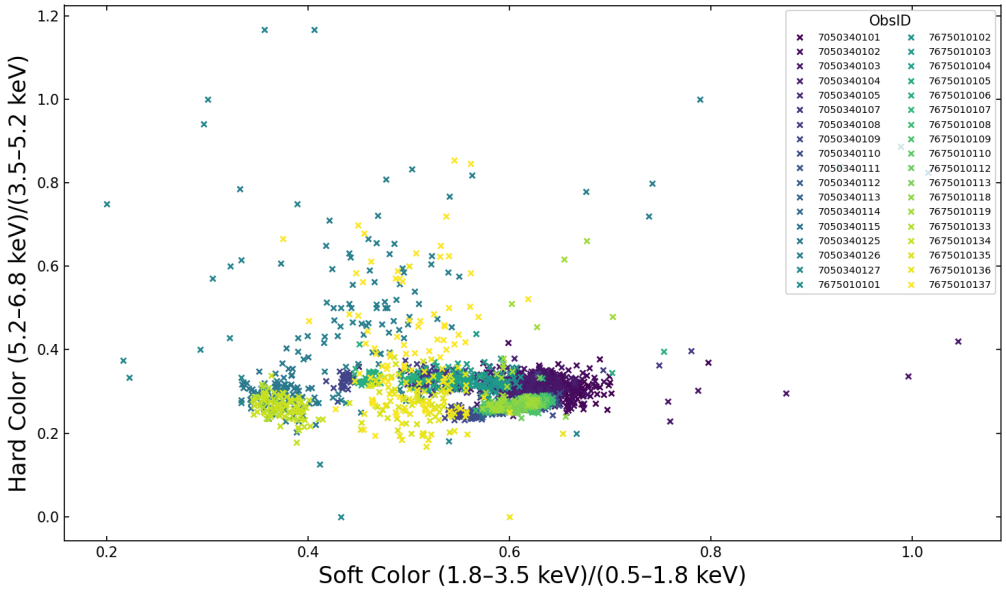

Figure 4.11: CCD of Aql X-1 during the 2024 outburst. The soft color is defined as the ratio (1.8-3.5 keV)/(0.5-1.8 keV), and the hard color as (5.2-6.8 keV)/(3.5-5.2 keV). Points are color-coded by ObsID.

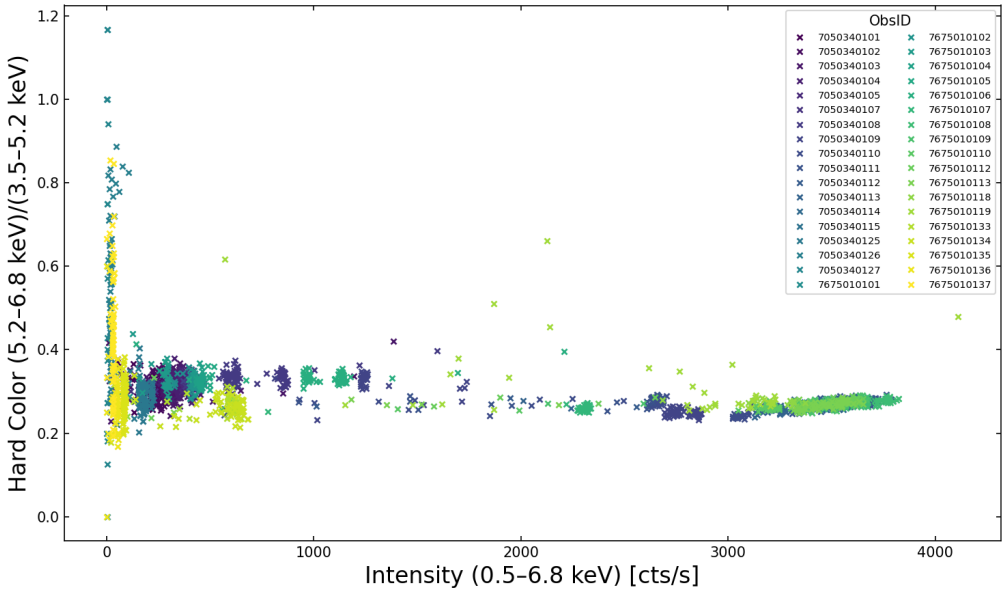

Figure 4.12: HID for the 2024 outburst. The hard color is plotted against the total intensity 0.5-6.8 keV band. Observations are color-coded by ObsID.

increases, producing a downward-sloping distribution. The majority of data points occupy a dense horizontal band at lower hardness values, while fewer points are seen at higher hardness. In the 2023 diagram, the spread in hardness is slightly larger, with individual points extending over a wider range of count rates. In contrast, the 2024 diagram shows a more compact sequence, with fewer points at the lowest intensities and a smoother overall distribution. Both HIDs display a consistent inverse relation between hardness and intensity across the observed data range.

4.6 Outburst Comparisons

A direct comparison of the 2023 and 2024 NICER-observed outbursts highlights both their shared characteristics and distinct quantitative differences. Both events exhibited the classical FRED morphology, each showing a rapid rise phase of approximately ten days followed by gradual decay. Spectral state transitions and consistent CCD tracks were observed in both outbursts, confirming similar overall evolution patterns. However, the specific flux profiles, durations, and spectral behaviors differ notably between the two epochs.

Light Curves: The 2023 outburst reached a higher peak flux of $\sim$3.2 ph s^{-1} cm^{-2} and lasted for about 50 days, while the 2024 outburst peaked at $\sim$2.0 ph s^{-1} cm^{-2} and lasted roughly 25 days. The 2023 event showed a smooth, exponential decay after a brief plateau, whereas the 2024 light curve displayed a flat-topped maximum and mild irregularities during its decay phase. Both exhibited rapid rise phases of comparable

duration, but the 2023 event maintained higher luminosity and stability over a longer interval.

Spectral Evolution: In both years, spectral fitting using `tbabs*nthcomp` provided statistically acceptable results (reduced $\chi^2 \approx$ 1-1.5). The column density $N_{\rm H}$ remained steady around (3-4.5) $\times 10^{21}$ cm^{-2}. During 2023, a gradual softening was evident, with the Γ increasing to $\sim$2.2-2.4 and the $kT_{\rm e}$ decreasing slightly near the peak. By contrast, the 2024 outburst remained spectrally harder, with $\Gamma \sim$ 1.6-1.8 and higher $kT_{\rm e}$ values, followed by only a modest softening during the decline. The $kT_{\rm bb}$ stayed within 0.4-0.8 keV in both events. These trends indicate that the 2023 outburst exhibited stronger spectral softening and a cooler Comptonizing component, while the 2024 event retained a harder, more compact emission spectrum.

Timing Results: No statistically significant millisecond pulsations were detected in either outburst. All Z_2^2 spectra were consistent with white-noise distributions, with no peaks surpassing the 99.9% confidence level. The highest observed powers ($Z_2^2 \approx$ 18-20) corresponded to $\lesssim 1\sigma$ significance and were not repeated in adjacent observations. Bootstrap simulations yielded a 3σ upper limit of $\sim$1.5% on the fractional rms amplitude, implying that any coherent pulsations must have been extremely weak or intermittent.

CCDs and HIDs: Both outbursts produced continuous CCD tracks spanning a wide range of soft color and a narrower range of hard color. The 2023 diagram showed a broader spread across intermediate soft color values, whereas the 2024 track was more compact with a denser grouping at lower hard color values. In the HIDs, an inverse relation between hardness and total count rate was observed in both years. The 2023 HID covered a wider hardness range with scattered points at high intensity, while the 2024 diagram showed a narrower, smoother distribution.

Chapter 5

Discussion

5.1 Spectral State Evolution

The NICER observations of Aql X-1 during the 2023 and 2024 outbursts reveal clear changes in spectral properties that reflect variations in the accretion flow around the neutron star. In both events, the spectra were well fitted by the thermal Comptonization model `tbabs*nthcomp`, showing that the observed emission is mainly produced when soft photons from the disk or boundary layer are up-scattered by hot electrons in a corona (Zdziarski et al., 1996; Done et al., 2007).

During the 2023 outburst (Figure 4.5), the photon index (Γ) gradually increased as the flux decreased, reflecting a spectral hardening of the source as the outburst faded. The photon index therefore serves primarily as a reference indicator of spectral state evolution, illustrating the transition from a softer, optically thick regime at higher luminosity to a harder, corona-dominated state at lower accretion rates. This behavior can be attributed to weaker Compton cooling of the corona when fewer soft photons are supplied from the accretion disk (Barret et al., 2000; Lin et al., 2007). The $kT_{\rm e}$ remained moderately high (a few keV) throughout, while the $kT_{\rm bb}$ stayed around 0.5-0.7 keV, suggesting that the soft emission region-likely the inner disk-did not vary strongly in temperature.

In the 2024 outburst, the Γ remained between 1.6 and 1.8, showing that the spectrum stayed consistently hard during the entire event. This, together with the shorter duration and lower intensity, implies that the system did not fully enter a soft or disk-dominated state. The results suggest that the corona stayed hotter and more dominant than in 2023, possibly because of a lower accretion rate and reduced cooling efficiency.

Overall, both outbursts follow the general pattern seen in many atoll-type neutron star systems (Hasinger and van der Klis, 1989). The 2023 event shows a clear soft-to-hard evolution, while the 2024 event remained mostly in the hard regime. This behavior points to the accretion rate as the main factor controlling spectral hardness and the balance between disk and coronal emission.

5.2 Comparison of the 2023 and 2024 Outbursts

The two outbursts have similar overall shapes, but their timescales and spectral evolution are very different. The 2023 outburst lasted longer (about 50-60 days) and had a higher peak flux. The 2024 event was shorter (about 40 days) with lower flux The light curves also show that 2023 had a smoother exponential decay, whereas the 2024 outburst exhibited a flat-topped maximum and mild variability during the decline.The CCDs and HIDs further highlight these differences. The data points in 2023 make a bigger track, which means that the source went through a wider range of spectral states. The distribution is tighter in 2024, which means that the source stayed within a small range of hardness. This means that the 2023 outburst had more dramatic changes in its spectrum, while the 2024 event was more stable and mostly hard

These differences can be naturally explained by changes in the amount of mass stored in the accretion disk before each event. In 2023, a bigger disk mass could have caused a longer, brighter outburst with a stronger soft component. In 2024, a smaller mass reservoir caused a shorter, harder event. These variations align with the thermal-viscous disk instability model (Lasota, 2001), which predicts that small changes in initial disk conditions can result in different outburst profiles without changing the basic mechanism.

5.3 Accretion Geometry and Emission Components

The spectral fits and parameter trends suggest that most of the X-ray emission during both outbursts came from a hot Comptonizing region, with a relatively steady soft-photon source from the inner disk. As the outburst faded, the decreasing accretion rate likely caused the corona to become hotter and more extended, leading to the observed spectral hardening. This is consistent with a geometry where the inner disk gradually recedes, giving the corona a larger volume and a stronger contribution to the total emission (Esin et al., 1997; Gilfanov, 2010).

5.4 Millisecond Pulsation Search

The search for coherent millisecond pulsations in both outbursts did not yield any significant detections. The search for coherent millisecond pulsations in both outbursts did not yield any significant detections. The Z_n^2 power spectra (computed with n=2) showed no peaks exceeding the 99.9 % confidence threshold, and the 3 σ upper limit on the fractional rms amplitude was about 1.5 %. This means that any pulsations present were too weak or too short-lived to be detected in the available data. The absence of pronounced pulsations indicates that the magnetic field of Aql X-1 was ineffective in directing the accretion flow during these high-accretion periods, aligning with prior observations of its intermittent pulsations (Casella et al., 2008; Bult et al., 2018; Campana et al., 2018).

5.5 Implications for Outburst Mechanisms

The observations show that both outbursts of Aql X-1 were triggered by the same physical process-the thermal-viscous instability in the accretion disk (Lasota, 2001; Hameury, 2020)-but developed differently because of changes in disk mass and irradiation. The 2023 outburst, with its longer duration and softer spectrum, likely involved a more massive and stable disk, while the 2024 outburst, shorter and harder, reflected a smaller or less efficiently heated disk. Despite these differences, the overall sequence of rise, peak, and decay, and the general correlation between flux and spectral hardness, remained consistent across both events.

This shows that Aql X-1 behaves as a stable recurrent atoll source, where each outburst follows the same physical cycle but with varying strength and duration depending on the disk conditions. The results highlight the importance of long-term monitoring to understand how changes in accretion rate and disk structure influence both spectral evolution and timing properties in transient neutron-star systems.

Chapter 6

Conclusions

6.1 Summary of Main Results

1. **Canonical state evolution:** Aql X-1 executed hard → soft → hard state cycles in both 2023 and 2024, with clear tracks in CCDs confirming atoll-source behavior and hysteresis.

2. **Coronal cooling at peak:** Spectra soften toward outburst maxima (larger Γ and reduced hardness), consistent with enhanced soft flux cooling the Comptonizing region and/or a smaller truncation radius of the inner disk.

3. **Stable absorption:** $N_{\rm H}$ remained consistent with interstellar values across epochs and between outbursts, with no strong evidence for variable local absorbers.

4. **Year-to-year differences:** The 2024 outburst was shorter and maintained a comparatively harder peak spectrum than 2023, plausibly reflecting a smaller disk mass reservoir and/or different irradiation efficiency.

5. **Model economy vs. completeness:** A simple `tbabs*nthcomp` model captured the gross spectral evolution with minimal degeneracy. Where curvature is weak, $kT_{\rm e}$ is not tightly constrained by NICER alone; our interpretation therefore emphasizes Γ, flux, and CCD morphology.

6.2 Astrophysical Implications

The repeatable sequence of spectral states and hysteresis supports a picture in which disk thermal-viscous instabilities trigger outbursts, while irradiation and coronal geometry regulate the detailed spectral balance. The softening at high flux indicates efficient

coupling between the inner disk/boundary layer and the corona, consistent with increased seed-photon supply and reduced coronal temperature/contrast. The modest differences between 2023 and 2024 highlight the sensitivity of the outburst morphology to initial disk conditions, but not to the underlying mechanism.

6.3 Future Work

Several targeted extensions would substantially sharpen the physical inferences:

1. **Broadband spectroscopy:** Coordinate *NuSTAR* (or similar) with NICER to constrain $kT_{\rm e}$ and optical depth, and to search for high-energy cutoffs that fix the coronal parameters.

2. **Reflection and geometry:** Add Fe K diagnostics and self-consistent reflection models (e.g. `relxillNS`/`relxillCp`) to probe inner-disk radius, inclination, and coronal height/compactness across states.

3. **Decomposing the soft excess:** Introduce `diskbb` and/or `bbody` components (with physically tied/untied seeds for `nthcomp`) where justified by residuals, to apportion flux between disk and boundary layer.

4. **Spectro-timing links:** Track fractional rms and QPO evolution in tandem with spectral parameters to map how coronal heating/cooling correlates with variability.

5. **Multiwavelength campaigns:** Optical/IR monitoring during rise/decay to quantify irradiation of the outer disk and to connect mass-transfer changes to X-ray state transitions; X-ray polarimetry (e.g. *IXPE*) in bright phases to constrain coronal geometry and scattering.

6. **Systematics control:** Cross-validate SCORPEON with contemporaneous background fields and alternate models; test small per-channel systematics in XSPEC; and standardize grouping/statistics across all epochs to ensure uniform comparability.

6.4 Closing Statement

Using two consecutive NICER-monitored outbursts, we established a coherent and repeatable portrait of Aql X-1's spectral evolution: a corona that softens under increasing soft-photon flux near peak, a disk/boundary-layer component that governs the spectral pivot, and a hysteretic loop across states that mirrors other atoll sources. Differences between 2023 and 2024 are quantitative rather than qualitative, consistent with varia-

tions in initial disk conditions and irradiation. With broadband coverage and refined component decompositions, Aql X-1 can continue to serve as a high-fidelity laboratory for the coupling between accretion disks, boundary layers, and Comptonizing coronae in neutron-star LMXBs.

Full Spectral Fit Tables

Table 6.1: Spectral parameters for Aql X-1 during the 2023 outburst fitted with `tbabs*nthcomp`. Uncertainties are 90% confidence intervals. A dagger (†) indicates parameters held fixed.

ID	MJD	*tbabs*	*nthcomp*			Flux
		$N_{\rm H}$ (10^{22} cm^{-2})	Γ	kT_e (keV)	$kT_{\rm seed}$ (keV)	$\log_{10} F$ (0.5–10 keV)
6634020101	60149.59084	$0.429^{+0.009}_{-0.009}$	$2.13^{+0.05}_{-0.07}$	926.53	$0.691^{+0.035}_{-0.046}$	$-9.2936^{+0.0021}_{-0.0021}$
6634020201	60150.04856	$0.373^{+0.006}_{-0.007}$	$1.99^{+0.04}_{-0.05}$	775.12	$0.726^{+0.019}_{-0.049}$	$-9.1569^{+0.0018}_{-0.0019}$
6634020301	60151.07986	$0.328^{+0.009}_{-0.008}$	$1.81^{+0.04}_{-0.04}$	4.45	$0.666^{+0.090}_{-0.070}$	$-8.9870^{+0.0019}_{-0.0020}$
6634020401	60152.11932	$0.313^{+0.013}_{-0.011}$	$1.67^{+0.02}_{-0.02}$	$2.74^{+0.22}_{-0.17}$	$0.447^{+0.055}_{-0.061}$	$-8.8177^{+0.0014}_{-0.0015}$
6634020501	60153.01501	$0.353^{+0.008}_{-0.011}$	$1.63^{+0.01}_{-0.01}$	$2.73^{+0.10}_{-0.08}$	0.147	$-8.6315^{+0.0013}_{-0.0012}$
6634020102	60154.75263	$0.299^{+0.009}_{-0.010}$	$1.66^{+0.01}_{-0.01}$	$3.27^{+0.22}_{-0.17}$	$0.204^{+0.036}_{-0.034}$	$-8.4705^{+0.0014}_{-0.0015}$
6634020104	60157.20368	$0.359^{+0.006}_{-0.006}$	$1.78^{+0.02}_{-0.02}$	$2.09^{+0.05}_{-0.04}$	$0.540^{+0.033}_{-0.031}$	$-7.8203^{+0.0010}_{-0.0010}$
6634020105	60158.23587	$0.372^{+0.009}_{-0.008}$	$1.67^{+0.01}_{-0.01}$	$1.89^{+0.03}_{-0.03}$	$0.444^{+0.037}_{-0.038}$	$-7.7120^{+0.0011}_{-0.0010}$
6634020106	60159.73981	$0.379^{+0.010}_{-0.009}$	$1.66^{+0.01}_{-0.01}$	$1.82^{+0.02}_{-0.02}$	$0.400^{+0.039}_{-0.039}$	$-7.6231^{+0.0010}_{-0.0010}$
6634020107	60160.17617	$0.382^{+0.012}_{-0.010}$	$1.65^{+0.01}_{-0.01}$	$1.80^{+0.02}_{-0.02}$	$0.374^{+0.042}_{-0.045}$	$-7.6032^{+0.0010}_{-0.0010}$
6634020108	60161.07384	$0.378^{+0.010}_{-0.008}$	$1.63^{+0.01}_{-0.01}$	$1.88^{+0.02}_{-0.02}$	$0.418^{+0.037}_{-0.044}$	$-7.5558^{+0.0009}_{-0.0010}$
6634020109	60162.10640	$0.381^{+0.010}_{-0.008}$	$1.63^{+0.01}_{-0.01}$	$1.86^{+0.02}_{-0.02}$	$0.399^{+0.038}_{-0.043}$	$-7.5592^{+0.0010}_{-0.0009}$
6634020110	60163.00969	$0.377^{+0.012}_{-0.009}$	$1.62^{+0.02}_{-0.02}$	$1.88^{+0.07}_{-0.06}$	$0.433^{+0.052}_{-0.058}$	$-7.5579^{+0.0011}_{-0.0012}$
6050340101	60163.91318	$0.365^{+0.009}_{-0.008}$	$1.67^{+0.02}_{-0.01}$	$1.98^{+0.05}_{-0.04}$	$0.484^{+0.045}_{-0.043}$	$-7.5732^{+0.0010}_{-0.0011}$
6050340102	60163.97777	$0.383^{+0.011}_{-0.010}$	$1.67^{+0.01}_{-0.01}$	$1.82^{+0.02}_{-0.02}$	$0.382^{+0.038}_{-0.042}$	$-7.6161^{+0.0010}_{-0.0010}$
6634020111	60164.19236	$0.374^{+0.011}_{-0.009}$	$1.63^{+0.01}_{-0.01}$	$1.88^{+0.04}_{-0.04}$	$0.423^{+0.044}_{-0.051}$	$-7.5722^{+0.0011}_{-0.0011}$
6634020112	60165.28727	$0.355^{+0.007}_{-0.006}$	$1.69^{+0.02}_{-0.02}$	$2.85^{+0.35}_{-0.24}$	$0.606^{+0.051}_{-0.050}$	$-7.5407^{+0.0011}_{-0.0011}$
6634020113	60166.10791	$0.376^{+0.013}_{-0.011}$	$1.67^{+0.02}_{-0.02}$	$1.83^{+0.05}_{-0.04}$	$0.412^{+0.052}_{-0.055}$	$-7.6163^{+0.0013}_{-0.0014}$
6050340103	60166.88242	$0.370^{+0.010}_{-0.008}$	$1.69^{+0.02}_{-0.01}$	$1.85^{+0.03}_{-0.03}$	$0.452^{+0.038}_{-0.042}$	$-7.6311^{+0.0011}_{-0.0011}$
6634020114	60167.21659	$0.379^{+0.009}_{-0.008}$	$1.71^{+0.01}_{-0.01}$	$1.87^{+0.02}_{-0.02}$	$0.424^{+0.032}_{-0.034}$	$-7.6453^{+0.0009}_{-0.0010}$
6634020115	60167.98729	$0.375^{+0.010}_{-0.008}$	$1.72^{+0.01}_{-0.01}$	$1.86^{+0.03}_{-0.03}$	$0.429^{+0.035}_{-0.038}$	$-7.6558^{+0.0011}_{-0.0011}$
6634020116	60169.01318	$0.456^{+0.004}_{-0.004}$	$1.64^{+0.01}_{-0.01}$	$1.88^{+0.02}_{-0.02}$	$0.024^{+0.055}_{-0.024}$	$-7.5822^{+0.0010}_{-0.0011}$
6634020117	60171.02824	$0.373^{+0.009}_{-0.008}$	$1.68^{+0.01}_{-0.01}$	$1.85^{+0.03}_{-0.03}$	$0.440^{+0.038}_{-0.040}$	$-7.6553^{+0.0011}_{-0.0011}$
6634020118	60172.00000	$0.370^{+0.009}_{-0.008}$	$1.71^{+0.01}_{-0.01}$	$1.94^{+0.04}_{-0.04}$	$0.457^{+0.035}_{-0.038}$	$-7.6624^{+0.0011}_{-0.0011}$
6634020119	60173.02098	$0.375^{+0.009}_{-0.008}$	$1.70^{+0.01}_{-0.01}$	$1.89^{+0.03}_{-0.03}$	$0.437^{+0.035}_{-0.037}$	$-7.6725^{+0.0010}_{-0.0010}$
6634020120	60174.18623	$0.376^{+0.009}_{-0.008}$	$1.67^{+0.01}_{-0.01}$	$1.91^{+0.03}_{-0.02}$	$0.433^{+0.035}_{-0.037}$	$-7.6533^{+0.0010}_{-0.0010}$
6634020121	60175.08993	$0.375^{+0.008}_{-0.008}$	$1.68^{+0.01}_{-0.01}$	$1.91^{+0.03}_{-0.02}$	$0.442^{+0.036}_{-0.033}$	$-7.6720^{+0.0010}_{-0.0009}$
6634020122	60176.31563	$0.370^{+0.008}_{-0.007}$	$1.69^{+0.01}_{-0.01}$	$1.98^{+0.04}_{-0.04}$	$0.479^{+0.035}_{-0.037}$	$-7.6723^{+0.0011}_{-0.0011}$
6634020123	60177.22662	$0.386^{+0.013}_{-0.012}$	$1.71^{+0.02}_{-0.01}$	$1.74^{+0.04}_{-0.03}$	$0.370^{+0.049}_{-0.048}$	$-7.7383^{+0.0013}_{-0.0013}$
6634020124	60178.19306	$0.360^{+0.009}_{-0.009}$	$1.71^{+0.02}_{-0.02}$	$2.17^{+0.09}_{-0.08}$	$0.516^{+0.048}_{-0.047}$	$-7.7009^{+0.0014}_{-0.0014}$
6634020125	60179.41435	$0.372^{+0.009}_{-0.008}$	$1.69^{+0.01}_{-0.01}$	$1.87^{+0.03}_{-0.03}$	$0.444^{+0.034}_{-0.038}$	$-7.7060^{+0.0011}_{-0.0010}$
6634020126	60180.33287	$0.374^{+0.008}_{-0.008}$	$1.68^{+0.01}_{-0.01}$	$1.94^{+0.03}_{-0.03}$	$0.439^{+0.036}_{-0.035}$	$-7.7315^{+0.0011}_{-0.0010}$
6634020127	60182.57662	$0.363^{+0.007}_{-0.007}$	$1.73^{+0.02}_{-0.02}$	$1.99^{+0.04}_{-0.04}$	$0.523^{+0.034}_{-0.034}$	$-7.7471^{+0.0011}_{-0.0010}$

Continued on next page

ID	MJD	*tbabs*	*nthcomp*			Flux
		$N_{\rm H}$ ($10^{22}\,{\rm cm}^{-2}$)	Γ	kT_e (keV)	$kT_{\rm seed}$ (keV)	$\log_{10} F$ (0.5–10 keV)
6634020128	60183.60532	$0.368^{+0.008}_{-0.008}$	$1.78^{+0.02}_{-0.02}$	$1.94^{+0.05}_{-0.05}$	$0.485^{+0.036}_{-0.036}$	$-7.8008^{+0.0012}_{-0.0012}$
6634020129	60184.19792	$0.369^{+0.007}_{-0.007}$	$1.73^{+0.02}_{-0.01}$	$1.94^{+0.04}_{-0.04}$	$0.496^{+0.036}_{-0.033}$	$-7.7684^{+0.0011}_{-0.0011}$
6634020130	60185.34745	$0.372^{+0.008}_{-0.007}$	$1.72^{+0.01}_{-0.01}$	$1.95^{+0.03}_{-0.03}$	$0.478^{+0.032}_{-0.034}$	$-7.7732^{+0.0010}_{-0.0010}$
6634020131	60186.40185	$0.290^{+0.011}_{-0.010}$	$1.74^{+0.02}_{-0.01}$	$1.91^{+0.05}_{-0.05}$	$0.316^{+0.013}_{-0.014}$	$-7.8440^{+0.0013}_{-0.0013}$
6634020132	60187.04745	$0.368^{+0.007}_{-0.007}$	$1.83^{+0.02}_{-0.02}$	$1.97^{+0.06}_{-0.05}$	$0.495^{+0.033}_{-0.032}$	$-7.8743^{+0.0011}_{-0.0012}$
6634020133	60188.01227	$0.367^{+0.008}_{-0.007}$	$1.79^{+0.02}_{-0.02}$	$2.03^{+0.06}_{-0.05}$	$0.503^{+0.035}_{-0.035}$	$-7.8471^{+0.0012}_{-0.0012}$
6634020134	60189.08678	$0.360^{+0.008}_{-0.008}$	$1.88^{+0.04}_{-0.03}$	$2.08^{+0.12}_{-0.10}$	$0.533^{+0.041}_{-0.039}$	$-7.8979^{+0.0014}_{-0.0014}$
6634020135	60190.05439	$0.361^{+0.007}_{-0.006}$	$1.85^{+0.02}_{-0.02}$	$2.14^{+0.07}_{-0.06}$	$0.545^{+0.032}_{-0.031}$	$-7.9035^{+0.0011}_{-0.0012}$
6634020136	60191.21529	$0.366^{+0.007}_{-0.007}$	$1.83^{+0.02}_{-0.02}$	$2.01^{+0.05}_{-0.05}$	$0.512^{+0.031}_{-0.030}$	$-7.9316^{+0.0011}_{-0.0011}$
6634020141	60196.05231	$0.366^{+0.007}_{-0.006}$	$2.04^{+0.03}_{-0.03}$	$2.38^{+0.15}_{-0.12}$	$0.508^{+0.026}_{-0.026}$	$-8.2000^{+0.0012}_{-0.0013}$
6634020142	60197.02514	$0.372^{+0.006}_{-0.006}$	$2.16^{+0.03}_{-0.02}$	$2.79^{+0.21}_{-0.16}$	$0.458^{+0.019}_{-0.019}$	$-8.3160^{+0.0012}_{-0.0012}$
6634020143	60198.77362	$0.379^{+0.008}_{-0.004}$	$2.27^{+0.04}_{-0.04}$	$3.39^{+0.72}_{-0.46}$	$0.432^{+0.020}_{-0.023}$	$-8.3889^{+0.0015}_{-0.0015}$
6634020144	60199.80979	$0.374^{+0.006}_{-0.006}$	$2.38^{+0.01}_{-0.04}$	589.89	$0.453^{+0.013}_{-0.015}$	$-8.4202^{+0.0013}_{-0.0012}$

Table 6.2: Spectral parameters for Aql X-1 during the 2024 outburst fitted with `tbabs*nthcomp`. Uncertainties are 90% confidence intervals. A dagger (†) indicates parameters held fixed.

ID	MJD	*tbabs*	*nthcomp*			Flux
		$N_{\rm H}$ (10^{22} cm^{-2})	Γ	kT_e (keV)	$kT_{\rm seed}$ (keV)	$\log_{10} F$ (0.5–10 keV)
7050340101	60573.66220	$0.325^{+0.006}_{-0.002}$	$1.83^{+0.03}_{-0.03}$	$4.80^{+1.05}_{-1.12}$	$0.834^{+0.032}_{-0.042}$	$-8.9155^{+0.0017}_{-0.0017}$
7050340102	60574.04779	$0.319^{+0.004}_{-0.005}$	$1.73^{+0.02}_{-0.02}$	$2.48^{+0.84}_{-0.00}$	$0.703^{+0.037}_{-0.037}$	$-8.8581^{+0.0014}_{-0.0014}$
7050340103	60575.01060	$0.312^{+0.009}_{-0.006}$	$1.60^{+0.01}_{-0.01}$	$1.64^{+0.98}_{-0.00}$	$0.549^{+0.022}_{-0.046}$	$-8.7190^{+0.0012}_{-0.0011}$
7050340104	60576.04039	$0.374^{+0.005}_{-0.004}$	$1.59^{+0.00}_{-0.00}$	$1.71^{+0.98}_{-0.00}$	$0.165^{+0.023}_{-0.035}$	$-8.6554^{+0.0012}_{-0.0012}$
7675010101	60576.74766	$0.369^{+0.012}_{-0.017}$	$1.59^{+0.01}_{-0.01}$	$2.65^{+0.15}_{-0.13}$	$0.186^{+0.068}_{-0.065}$	$-8.6366^{+0.0019}_{-0.0020}$
7050340105	60577.00796	$0.363^{+0.019}_{-0.031}$	$1.59^{+0.02}_{-0.01}$	$2.43^{+0.18}_{-0.14}$	0.000	$-8.6253^{+0.0027}_{-0.0028}$
7675010102	60577.07250	$0.365^{+0.010}_{-0.018}$	$1.59^{+0.01}_{-0.01}$	$2.60^{+0.11}_{-0.10}$	$0.181^{+0.075}_{-0.060}$	$-8.6253^{+0.0017}_{-0.0017}$
7675010103	60578.03547	$0.348^{+0.010}_{-0.012}$	$1.59^{+0.01}_{-0.01}$	$2.88^{+0.16}_{-0.13}$	$0.193^{+0.048}_{-0.048}$	$-8.5287^{+0.0016}_{-0.0016}$
7675010104	60579.00370	$0.333^{+0.010}_{-0.012}$	$1.59^{+0.01}_{-0.01}$	$2.93^{+0.16}_{-0.13}$	$0.200^{+0.045}_{-0.043}$	$-8.4413^{+0.0015}_{-0.0016}$
7050340107	60579.13657	$0.336^{+0.009}_{-0.011}$	$1.59^{+0.01}_{-0.01}$	$2.99^{+0.17}_{-0.14}$	$0.204^{+0.043}_{-0.042}$	$-8.4819^{+0.0016}_{-0.0016}$
7675010105	60580.04044	$0.312^{+0.014}_{-0.015}$	$1.59^{+0.01}_{-0.01}$	$3.04^{+0.31}_{-0.23}$	$0.215^{+0.055}_{-0.060}$	$-8.4110^{+0.0024}_{-0.0023}$
7050340108	60580.68727	$0.302^{+0.007}_{-0.008}$	$1.56^{+0.00}_{-0.00}$	$2.95^{+0.08}_{-0.08}$	$0.217^{+0.031}_{-0.029}$	$-8.3094^{+0.0011}_{-0.0012}$
7050340109	60581.46191	$0.363^{+0.007}_{-0.006}$	$1.94^{+0.02}_{-0.01}$	$2.65^{+0.10}_{-0.09}$	$0.442^{+0.022}_{-0.022}$	$-7.9879^{+0.0010}_{-0.0011}$
7050340110	60582.23773	$0.368^{+0.007}_{-0.006}$	$1.74^{+0.01}_{-0.01}$	$1.92^{+0.03}_{-0.03}$	$0.484^{+0.029}_{-0.032}$	$-7.7679^{+0.0010}_{-0.0010}$
7675010107	60582.36505	$0.370^{+0.008}_{-0.007}$	$1.77^{+0.02}_{-0.01}$	$1.93^{+0.04}_{-0.03}$	$0.455^{+0.031}_{-0.031}$	$-7.7899^{+0.0010}_{-0.0011}$
7050340111	60583.06991	$0.374^{+0.008}_{-0.007}$	$1.70^{+0.01}_{-0.01}$	$1.92^{+0.03}_{-0.02}$	$0.442^{+0.031}_{-0.032}$	$-7.7425^{+0.0010}_{-0.0010}$
7675010108	60583.39755	$0.373^{+0.008}_{-0.007}$	$1.70^{+0.01}_{-0.01}$	$1.94^{+0.03}_{-0.03}$	$0.447^{+0.031}_{-0.034}$	$-7.7341^{+0.0010}_{-0.0010}$
7050340112	60584.04311	$0.369^{+0.007}_{-0.007}$	$1.74^{+0.01}_{-0.01}$	$1.97^{+0.03}_{-0.03}$	$0.476^{+0.031}_{-0.030}$	$-7.7646^{+0.0010}_{-0.0010}$
7675010109	60584.75282	$0.370^{+0.007}_{-0.007}$	$1.72^{+0.01}_{-0.01}$	$1.94^{+0.03}_{-0.03}$	$0.485^{+0.032}_{-0.031}$	$-7.7555^{+0.0010}_{-0.0010}$
7050340113	60585.01113	$0.371^{+0.008}_{-0.007}$	$1.77^{+0.02}_{-0.01}$	$1.94^{+0.04}_{-0.03}$	$0.457^{+0.031}_{-0.031}$	$-7.7956^{+0.0011}_{-0.0010}$
7675010110	60585.84999	$0.371^{+0.008}_{-0.007}$	$1.77^{+0.01}_{-0.01}$	$1.92^{+0.03}_{-0.03}$	$0.441^{+0.030}_{-0.031}$	$-7.7998^{+0.0010}_{-0.0011}$
7050340114	60586.69071	$0.367^{+0.008}_{-0.007}$	$1.72^{+0.02}_{-0.01}$	$1.88^{+0.04}_{-0.03}$	$0.476^{+0.035}_{-0.036}$	$-7.7586^{+0.0011}_{-0.0011}$
7675010112	60587.20741	$0.369^{+0.008}_{-0.008}$	$1.71^{+0.01}_{-0.01}$	$1.98^{+0.04}_{-0.03}$	$0.459^{+0.036}_{-0.033}$	$-7.7440^{+0.0011}_{-0.0011}$
7675010113	60588.43219	$0.370^{+0.008}_{-0.007}$	$1.73^{+0.01}_{-0.01}$	$1.89^{+0.03}_{-0.03}$	$0.460^{+0.030}_{-0.033}$	$-7.7694^{+0.0011}_{-0.0010}$
7050340115	60588.87338	$0.369^{+0.010}_{-0.009}$	$1.74^{+0.02}_{-0.02}$	$1.90^{+0.06}_{-0.05}$	$0.465^{+0.041}_{-0.043}$	$-7.7734^{+0.0013}_{-0.0013}$
7675010118	60593.41088	$0.354^{+0.008}_{-0.007}$	$1.76^{+0.03}_{-0.02}$	$2.13^{+0.09}_{-0.08}$	$0.546^{+0.043}_{-0.043}$	$-7.7938^{+0.0013}_{-0.0012}$
7675010119	60594.11920	$0.362^{+0.011}_{-0.010}$	$1.74^{+0.05}_{-0.04}$	$1.90^{+0.30}_{-0.17}$	$0.465^{+0.067}_{-0.063}$	$-7.8248^{+0.0013}_{-0.0012}$

Bibliography

Arnaud, K. A. (1996). Xspec: The first ten years. In Jacoby, G. H. and Barnes, J., editors, *Astronomical Data Analysis Software and Systems V*, volume 101 of *ASP Conference Series*, page 17.

Asai, K., Matsuoka, M., Mihara, T., Sugizaki, M., Serino, M., and Negoro, H. (2013). Classification of outbursts in aql x-1 based on maxi observations. *Publications of the Astronomical Society of Japan*, 65(2):29.

Bahramian, A. and Degenaar, N. (2023). Low-Mass X-ray Binaries. In *Handbook of X-ray and Gamma-ray Astrophysics*, page 120.

Barret, D., Olive, J. F., Boirin, L., Done, C., Skinner, G. K., and Grindlay, J. E. (2000). The spectral states of neutron-star low-mass x-ray binaries: Bepposax observations of 4u 1705–44. *The Astrophysical Journal*, 533:329–351.

Belloni, T. M. (2010). States and transitions in black hole binaries. In Belloni, T., editor, *The Jet Paradigm*, volume 794 of *Lecture Notes in Physics*, pages 53–84. Springer, Berlin, Heidelberg.

Buccheri, R., Bennett, K., Bignami, G. F., Bloemen, J. B. G. M., Boriakoff, V., Caraveo, P. A., Hermsen, W., Kanbach, G., Manchester, R. N., Masnou, J. L., Mayer-Hasselwander, H. A., Ozel, M. E., Paul, J. A., Sacco, B., Scarsi, L., and Strong, A. W. (1983). Search for pulsed gamma-ray emission from radio pulsars in the cos-b data. *Astronomy and Astrophysics*, 128:245–251.

Bult, P., Arzoumanian, Z., Cackett, E. M., Chakrabarty, D., Gendreau, K. C., Guillot, S., Homan, J., Jaisawal, G. K., Keek, L., Kenyon, S., Lamb, F. K., Ludlam, R., Mahmoodifar, S., Markwardt, C., Miller, J. M., Prigozhin, G., Soong, Y., Strohmayer, T. E., and Uttley, P. (2018). A NICER Look at the Aql X-1 Hard State. , 859(1):L1.

Bult, P. and van der Klis, M. (2015). Intermittent accretion-powered pulsations and the spin evolution of aql x-1. *Astrophysical Journal*, 806(1):90.

Campana, S., Coti Zelati, F., and D'Avanzo, P. (2014). The 2013 outburst of aql x-1. *Monthly Notices of the Royal Astronomical Society*, 441(3):1984–1991.

Campana, S., Di Salvo, T., D'Avanzo, P., Papitto, A., Stella, L., D'Elia, V., and Burderi, L. (2018). A decade of transitional millisecond pulsars: A review. *Astronomy and Astrophysics Review*, 26(1):7.

Casella, P., Altamirano, D., Patruno, A., Wijnands, R., and van der Klis, M. (2008). Discovery of intermittent millisecond x-ray pulsations in aql x-1. *The Astrophysical Journal Letters*, 674(1):L41–L44.

Done, C., Gierliński, M., and Kubota, A. (2007). Modelling the behaviour of accretion flows in x-ray binaries. *Astronomy and Astrophysics Review*, 15:1–66.

Esin, A. A., McClintock, J. E., and Narayan, R. (1997). Advection-dominated accretion and the spectral states of black hole x-ray binaries: Application to nova muscae 1991. *The Astrophysical Journal*, 489:865–889.

Fender, R. P., Belloni, T. M., and Gallo, E. (2004). Towards a unified model for black hole x-ray binary jets. *Monthly Notices of the Royal Astronomical Society*, 355(4):1105–1118.

Frank, J., King, A., and Raine, D. (2002). *Accretion Power in Astrophysics*. Cambridge University Press, Cambridge, 3 edition.

Galloway, D. K., Muno, M. P., Hartman, J. M., Psaltis, D., and Chakrabarty, D. (2008). Thermonuclear (type i) x-ray bursts observed by rxte. *The Astrophysical Journal Supplement Series*, 179(2):360–422.

Gendreau, K. C., Arzoumanian, Z., and Okajima, T. (2016). The neutron star interior composition explorer (nicer): mission definition. *Proceedings of SPIE*, 9905:99051H.

Gilfanov, M. (2010). X-ray emission from black-hole binaries. *Lecture Notes in Physics*, 794:17–51.

Güngör, C., Güver, T., and Ekşi, K. Y. (2014). Classification and spectral evolution of outbursts of Aql X-1. , 439(3):2717–2727.

Hameury, J.-M. (2020). The disk instability model for dwarf novae and low-mass x-ray binary transients. *Advances in Space Research*, 66(4):1004–1025.

Hasinger, G. and van der Klis, M. (1989). Two patterns of correlated x-ray timing and spectral behaviour in low-mass x-ray binaries. *Astronomy and Astrophysics*, 225:79–96.

Homan, J., Wijnands, R., van der Klis, M., Belloni, T., van Paradijs, J., Klein-Wolt, M., Fender, R., and Méndez, M. (2001). Rossi x-ray timing explorer observations of the neutron star x-ray transient aquila x-1 during the 2000 outburst decay. *The Astrophysical Journal Supplement Series*, 132(2):377–402.

Huppenkothen, D., Bachetti, M., Stevens, A. L., Migliari, S., Balm, P., Hammad, F., Kara, E., Markwardt, C. B., Migliari, S., Strohmayer, T., and Vaughan, S. (2019). Stingray: A modern python library for spectral timing. *The Astrophysical Journal*, 881:39.

Lasota, J.-P. (2001). The disc instability model of dwarf novae and low-mass x-ray binary transients. *New Astronomy Reviews*, 45(7):449–508.

Lewin, W. H. G., van Paradijs, J., and van den Heuvel, E. P. J., editors (1995). *X-ray Binaries*. Cambridge University Press, Cambridge.

Lin, D., Remillard, R. A., and Homan, J. (2007). Evaluating spectral models for black hole x-ray binaries in the thermal dominant state. *The Astrophysical Journal*, 667:1073–1086.

Maccarone, T. J. and Coppi, P. S. (2003). Hysteresis in the light curves of black hole x-ray binaries. *Monthly Notices of the Royal Astronomical Society*, 338(1):189–196.

Maitra, D. and Bailyn, C. D. (2008). The spectral states and long-term behavior of aql x-1. *The Astrophysical Journal*, 688(1):537–549.

Migliari, S. and Fender, R. P. (2006). Jets in neutron star x-ray binaries: a comparison with black holes. *Monthly Notices of the Royal Astronomical Society*, 366(1):79–91.

Muñoz-Darias, T., Jiménez-Ibarra, F., Armas Padilla, M., et al. (2022). The optical/x-ray evolution of aquila x-1. *Monthly Notices of the Royal Astronomical Society*, 512(2):2102–2115.

NASA/GSFC (2024). Heasoft and nicerdas documentation. https://heasarc.gsfc.nasa.gov/docs/software/heasoft/. NASA Goddard Space Flight Center (GSFC).

NICER Team (2024). Nicer background models: Scorpeon and 3c50. NASA/GSFC Documentation. https://heasarc.gsfc.nasa.gov/docs/nicer/analysis_threads/.

Patruno, A. and Watts, A. L. (2021). *Accreting Millisecond X-ray Pulsars*, volume 461 of *Astrophysics and Space Science Library*. Springer Nature.

Putha, K. G., Bhargava, Y., and Bhattacharyya, S. (2024). Probing outbursts of the transient neutron star low-mass X-ray binary Aql X-1 with NICER: a study of spectral evolution. , 532(4):3961–3971.

Sazonov, S., Khabibullin, I., Medvedev, P., and Sunyaev, R. (2020). The galactic lmxb population and the galactic centre region. *Monthly Notices of the Royal Astronomical Society*, 497(1):648–667.

van der Klis, M. (2006). Rapid x-ray variability. In Lewin, W. H. G. and van der Klis, M., editors, *Compact Stellar X-ray Sources*, pages 39–112. Cambridge University Press, Cambridge.

Verner, D. A., Ferland, G. J., Korista, K. T., and Yakovlev, D. G. (1996). Atomic data for astrophysics. ii. new analytic fits for photoionization cross sections of atoms and ions. *The Astrophysical Journal*, 465:487–498.

Wijnands, R. and van der Klis, M. (1998). A millisecond pulsar in an x-ray binary system. *Nature*, 394:344–346.

Wilms, J., Allen, A., and McCray, R. (2000). On the absorption of x-rays in the interstellar medium. *The Astrophysical Journal*, 542:914–924.

Zdziarski, A. A., Johnson, W. N., and Magdziarz, P. (1996). Broad-band γ-ray and x-ray spectra of ngc 4151 and their implications for physical processes and geometry. *Monthly Notices of the Royal Astronomical Society*, 283:193–206.

Życki, P. T., Done, C., and Smith, D. A. (1999). Thermal comptonization and reflection in the x-ray spectra of seyfert galaxies and galactic black hole candidates. *Monthly Notices of the Royal Astronomical Society*, 309:561–575.